AD-A144 436 ANALYSIS OF COMBUSTION OSCILLATIONS IN HETEROGENEOUS SYSTEMS(U) PRINCETON COMBUSTION RESEARCH LABS INC NJ M BEN-REUVEN ET AL. NOV 83 PCRL-FR-83-005 1/1

UNCLASSIFIED AFOSR-TR-84-0700 F49620-82-C-0062 F/G 21/2 NL

END

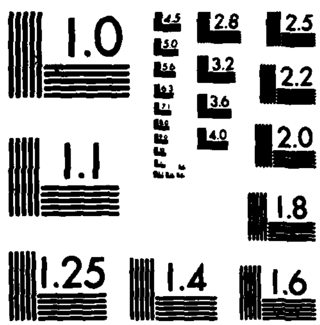

MICROCOPY RESOLUTION TEST CHART

NATIONAL BUREAU OF STANDARDS-1963-A

AFOSR-TR- 84-0700

AD-A144 436

PRINCETON COMBUSTION RESEARCH LABORATORIES, INC.

ANALYSIS OF COMBUSTION OSCILLATIONS

IN HETEROGENEOUS SYSTEMS

Contract No. F49620-82-C-0062

DTIC FILE COPY

DTIC
ELECTE
AUG 1 7 1984
S A

PRINCETON COMBUSTION RESEARCH LABORATORIES, INC.
1041 U.S. Highway One North, Princeton, New Jersey 08540 Telephone (609) 452-9200

84 08 16 036

Report No. PCRL-FR-83-005
November 1983

ANALYSIS OF COMBUSTION OSCILLATIONS IN HETEROGENEOUS SYSTEMS

Contract No. F49620-82-C-0062

Submitted to

Air Force Office of Scientific Research
ATTN: AFOSR/NA (Dr. Leonard H. Caveny)
Building 410
Bolling Air Force Base, DC 20332

Submitted by

Moshe Ben-Reuven and Martin Summerfield
Princeton Combustion Research Laboratories, Inc.
475 U.S. Highway One
Monmouth Junction, NJ 08852

November 1983

UNCLASSIFIED

SECURITY CLASSIFICATION OF THIS PAGE (When Data Entered)

REPORT DOCUMENTATION PAGE

READ INSTRUCTIONS BEFORE COMPLETING FORM

1. REPORT NUMBER: AFOSR-TR- 84-0700
2. GOVT ACCESSION NO.: AD-A144436
3. RECIPIENT'S CATALOG NUMBER:
4. TITLE (and Subtitle): Analysis of Combustion Oscillations in Heterogeneous Systems
5. TYPE OF REPORT & PERIOD COVERED: Final Report, 15 Mar 82 - 14 Mar 83
6. PERFORMING ORG. REPORT NUMBER: PCRL-FR-83-005
7. AUTHOR(s): Dr. Moshe Ben-Reuven, Dr. Martin Summerfield
8. CONTRACT OR GRANT NUMBER(s): F49620-82-C-0062
9. PERFORMING ORGANIZATION NAME AND ADDRESS: Princeton Combustion Research Laboratories, Inc., 475 U.S. Highway One, Monmouth Junction, NJ 08852
10. PROGRAM ELEMENT, PROJECT, TASK AREA & WORK UNIT NUMBERS: 61102F, 2308/A1
11. CONTROLLING OFFICE NAME AND ADDRESS: AFOSR/NA, Bolling AFB, DC 20332
12. REPORT DATE: November 1983
13. NUMBER OF PAGES: 60
14. MONITORING AGENCY NAME & ADDRESS (if different from Controlling Office):
15. SECURITY CLASS. (of this report): Unclassified
15a. DECLASSIFICATION DOWNGRADING SCHEDULE:
16. DISTRIBUTION STATEMENT (of this Report): Distribution Unlimited.

Approved for public release; distribution unlimited.

17. DISTRIBUTION STATEMENT (of the abstract entered in Block 20, if different from Report):
18. SUPPLEMENTARY NOTES:
19. KEY WORDS (Continue on reverse side if necessary and identify by block number): Solid propellant rocket motors; solid propellants, velocity-coupling; combustion instability; acoustic/viscous interaction; nonsteady reacting flow; core-combustion/acoustic coupling; internal rocket flowfields; cold flow simulation; injected viscous wall layer.
20. ABSTRACT (Continue on reverse side if necessary and identify by block number)

SUMMARY

This analysis is aimed at the near-wall processes in an injected, axisymmetric, viscous flow. It is a part of an overall study of solid propellant rocket instability, in which cold flow simulation is evaluated as a tool to elucidate possible instability-driving mechanisms. One such prominent mechanism

(CONTINUED . . .)

seems to be visco-acoustic coupling, as indicated by earlier detailed order of magnitude analysis. The major component of the overall study involves numerical simulation of the full set of coreflow equations of motion (nonsteady, axisymmetric) by a modified MacCormack integration technique. To clarify some of the physical interactions inherent in the various regimes of the flowfield, two (separate) singular perturbation analyses have been carried out. The head-end boundary regime, and the injected sidewall layer, both involve appreciable viscous dissipation, and hence are characterized by predominantly parabolic differential systems. The inverse square root of the injection Reynolds number serves as a small-perturbation quantity. The sidewall layer analysis yields a first order axial pressure distribution (due to viscous effects) which correlates the available steady state data (CSD experiments, 1982) very well. The radial dependence of the inner variables up to first order is solved, so that the (x,t) dependence can be described by much simpler partial differential systems; inner/outer matching was not attempted. The finite-difference coreflow algorithm is described, and a source listing from one preliminary version (ROSCO-2) is provided. Convergence to steady state has been achieved with this program recently (by marching forward in time from imposed initial data). The modular structure of the computer program facilitates addition of special segments (such as two-equation turbulence modeling).

Acknowledgment

This research was sponsored by the Air Force Office of Scientific Research (AFSC), under Contract F49620-81-C-0018. The United States Government is authorized to reproduce and distribute reprints for governmental purposes notwithstanding any copyright notation hereon.

Technical cognizance for this contract was provided at Air Force Office of Scientific Research, Bolling AFB, by Dr. Leonard H. Caveny, Program Manager, Aerospace Sciences.

TABLE OF CONTENTS

SUMMARY

This analysis is aimed at the near-wall processes in an injected, axisymmetric, viscous flow. It is a part of an overall study of solid propellant rocket instability, in which cold flow simulation is evaluated as a tool to elucidate possible instability-driving mechanisms. One such prominent mechanism seems to be visco-acoustic coupling, as indicated by earlier detailed order of magnitude analysis. The major component of the overall study involves numerical simulation of the full set of coreflow equations of motion (nonsteady, axisymmetric) by a modified MacCormack integration technique. To clarify some of the physical interactions inherent in the various regimes of the flowfield, two (separate) singular perturbation analyses have been carried out. The head-end boundary regime, and the injected sidewall layer, both involve appreciable viscous dissipation, and hence are characterized by predominantly parabolic differential systems. The inverse square root of the injection Reynolds number serves as a small-perturbation quantity. The sidewall layer analysis yields a first order axial pressure distribution (due to viscous effects) which correlates the available steady state data (CSD experiments, 1982) very well. The radial dependence of the inner variables up to first order is solved, so that the (x,t) dependence can be described by much simpler partial differential systems; inner/outer matching was not attempted. The finite-difference coreflow algorithm is described, and a source listing from one preliminary version (ROSCO-2) is provided. Convergence to steady state has been achieved with this program recently (by marching forward in time from imposed initial data). The modular structure of the computer program facilitates addition of special segments (such as two-equation turbulence modeling).

1. BACKGROUND

This is part of a study aimed at elucidation of the physical mechanisms capable of driving acoustic instability in solid propellant motors, particularly of the type termed velocity-coupled instability. Previous studies on the coupling between velocity oscillations and the combustion process in solid propellant motors have demonstrated the complexity of the overall phenomenon, but have not yet defined the basic mechanisms nor how they operate under flow conditions prevailing in rocket chambers. Critical literature review and order of magnitude analyses of velocity coupling mechanisms have been carried out, including visco-acoustic coupling and turbulence combustion coupling. The major goal of the study is the analytical simulation of the interior flow field within a solid propellant grain. The focus is on the Stokes layer, with the objective of investigating the particular instability mechanism of visco-acoustic coupling. Preliminary analysis has indicated that this mechanism is both plausible and sufficiently powerful to drive nonlinear vibrations; it has been shown that the frequency-dependent surface heat feedback component, due to viscous/acoustic coupling, has both phase amplitude ranges which would enable driving of acoustic vibrations; its amplitude tends to increase as the mean coreflow Mach number and the frequency become higher. A comprehensive analytical model of the flow field within the viscous wall layer region has been derived, for an axisymmetric, nonsteady flow field configuration. For a simulation of the cold flow test results gnerated at UTC/CSD, four conservation equations are incorporated for continuity, momentum and energy.

The major aspect of the near-wall behavior from the visco-acoustic point of view, is the laminar dissipative processes typical to that region. This analysis is focused on the near-wall processes. Although the solultions derived are nonsteady in general, the radial wall-layer distributions obtained could best be demonstrated at steady state. For this reason, the review herein is limited to steady behavior.

Culick [1] derived a solution to the Stokes stream function equation or flow in a pipe with injected sidewalls. The flow is rotational, and despite being inviscid, could obtain a solution for the axial velocity component which satisfied the no-slip boundary condition at the wall. The solution which satisfies the boundary data, namely, $u(x=0)=0$, $u(r=1)=0$, and $v(r=1)=1$, yields:

$$V = -\sin\left(\frac{\pi}{2}r^2\right)/r, \qquad u = \pi x \cos\left(\frac{\pi}{2}r^2\right)$$

Of the general family of solutions obtainable, only that which allows full determination of the vorticity (the azymuthal component alone remains) by the available boundary data, is physically meaningful; the rest were therefore rejected. The axial pressure distribution obtained from the momentum equation is parabolic,

$$(P_0 - P)/\rho v^2 = \frac{\pi}{2} x^2$$

This type of injected flow field has been investigated previously both experimentally and theoretically. In particular the early theoretical work of Berman [2], who arrived at a power-series solution to the perturbation problem of suction in a prismatic, porous-walled channel, with the suction Reynolds number serving as small-perturbation quantity. The analytical results of G. Taylor [3] and Wageman and Guevara [4] more closely resemble the cosine terms of Culick [1]; both [3,4] have carried out experiments as well, and both demonstrated very good agreement between the measured axial velocity profiles and the calculated ones. It appears that Culick [1] has arrived at his results independently, since no reference was made to any of the previous works. In the experiments by Dunlap, Willoughby and Hermsen [5], the formulation derived by Culick [1] was used to correlate the measured data, again with considerable success, regarding the coreflow axial velocity profile, that is, away from the close neighborhood of the wall.

Other experiments by Olson and Eckert [6] and later by Huesman and Eckert [7] tend likewise to verify the validity of this formulation, in particular regarding the radial velocity profile, which indeed exhibits a peak near the porous surface [6], as well as the axial pressure distribution (the latter shown as a linear correltaion between the friction coefficient, C_f, and the inverse mean axial velocity, which are both proportional to $1/x$.

The recent (and ongoing) experimental study by Brown, et al [8] provides valuable information regarding the steady state axial pressure profile and the axial velocity distribution, as well as nonsteady wall heat transfer (obtained by exciting the standing acoustic modes in the tube). Departure of the steady state data from the predictions of the aforementioned formulation by Culick [1] was attributed to possible transition to turbulence. As will be shown in this study, the pressure data obtained can be simulated very well with a first-order pressure perturbation, arising from the **laminar** viscous wall-layer analysis.

Earlier, Yagodkin [9] reported an experimental cold flow setup, with an injected porous pipe. The maximal injection Reynolds number was 250, which is 2-3 orders of magnitude less than that corresponding to actual internal rocket flows. Hot-wire anemometry was used to obtain axial velocity and axial velocity fluctuation vs axial and radial distance. Turbulence intensity seems to peak near the surface, and decrease toward the centerline and toward the pipe wall. These observations are qualitatively similar to those obtained later by Yamada, et al [10]. Although a transition region, at R_{eo}=100-150, was speculated [9] to involve "large eddy structures", no such evidence appears in the experimental data reported [9].

Further studies by Yagodkin, with Varapaev [11] and Sviridenkov [12] are theoretical, and address the problem of laminar stability of injected channel flows, i.e., transition to turbulence. Thus, modified versions of the Orr-Sommerfield problem were investigated analytically [11] and numerically [12]. Two related laminar flow stability analyses are by Goldshtik, et al [13] and Alekseev, et al [14]. None of these theoretical analyses indicates the presence of large turbulent eddy structures prior to a full transition point, neither do they obtain an origin of such turbulence on the centerline upstream.

Recently Flandro [15] has carried out a theoretical analysis for a burning propellant in a cylindrical grain, under the effect of incident acoustic waves. A detailed formulation was derived with a double expansion, in terms of both inverse Reynolds number as well as Mach number (independent small parameters). A nonsteady premixed combustion zone was considered near the propellant surface; the assumption is made, however, that flow within the combustion zone is pure radial, i.e., zero axial component to all orders. Thus it could be anticipated that the results resemble (regarding nonsteady combustion behavior) those of T'ien [16], and there seems to be only small differences between the response to tangent and to perpendicular wave incedence. The problem is finally solved numerically, and details of the inner/outer matching process were not given.

2. ANALYTICAL MODEL OF THE COREFLOW

2.0 INTRODUCTION

In this chapter, the equations of motion pertaining to the core-flow simulation are presented, for an axisymmetric flow field. Turbulence and combustion are precluded from the present formulation, for reasons discussed earlier. Other than these simplifications, the full compressible, nonsteady, viscous equations of motion are considered, with all the dissipative terms included. A schematic of the simulated flowfield with the various regions of interest is shown in Figure 1.

Treatment is divided into three subsections, in which the coreflow region, the head-end closure region, and the porous, injection sidewall region, are discussed in detail. The latter two parts represent singular perturbation analyses of the boundary-layer type, which are incorporated for generation of boundary data within the coreflow solution procedure. Important physical insights are obtained regarding the behavior of the system at relatively large injection Reynolds numbers, coupled with low injected Mach numbers, such that

$$M_o{}^2 \sim O(1/R_{eo})$$

The numerical algorithm developed for solution of the coreflow differential system is a modified MacCormack scheme. Its finite differencing details are discussed in the next chapter, along with a current listing of the Fortran code.

2.1 THE COREFLOW FORMULATION

The objective is to simulate the cold-flow experiments of Dr. Brown at UTC/CSD, which utilize cylindrical geometry. For this purpose, an axisymmetric formulation was derived, to describe a nonsteady, compressible, viscous flowfield. For the coreflow region, with typical injection Reynolds numbers of order 1000 and larger, we assumed constant and uniform thermophysical properties. As mentioned earlier, combustion (or chemical change) and turbulence are precluded at the present stage.

The five equations of motion, for continuity, radial momentum, axial momentum and energy are presented in differential form. A caloric equation of state (pertaining to perfect gas) completes the model to form closure of the dependent variables.

The following dimensionless independent variables are introduced, based on the two physical scales of reference, inner chamber radius, R_o^*, and reference injection velocity, v_o^*:

$$r = r^*/R_o^*, \quad x = x^*/R_o^*, \quad t = t^*/t_o^* \tag{2.1}$$

where

$$t_o^* = R_o^*/v_o^* \tag{2.2}$$

The dependent variables are:

$$\rho = \rho^*/\rho_o^*, \quad v = v^*/v_o^*, \quad u = u^*/v_o^*, \quad h_o = h^*/h_o^*$$

and

$$p = p^*/P_o^* \tag{2.3}$$

In the last equations, the properties used for non-dimensionalization are the reference (injected) density, ρ_o^*, and the reference chamber pressure, p_o^*; the corresponding thermal enthalpy, h_o^*, is calculated from the caloric equation of state,

$$p_o^* = \frac{\gamma-1}{\gamma}\rho_o^* h_o^* \tag{2.4}$$

where γ =Cp/Cv is the specific heat ratio, is considered as constant. The reference speed of sound is

$$a_o^* = (\gamma p_o^*/\rho_o^*)^{1/2} = \sqrt{(\gamma-1)h_o^*} \tag{2.5}$$

The corresponding injection Mach number is

$$M_o = v_o^*/a_o^* \tag{2.6}$$

The reference (injection) Reynolds number and Prandtl number are, respectively,

$$R_{eo} = \rho_o^* V_o^* R_o^* / \mu^* \tag{2.7}$$

$$P_r = \mu^* c_p^* / \lambda^* \tag{2.8}$$

Recall that the viscosity, thermal conductivity and isobaric specific heat are all uniform and constant within the present cold-flow simulation. These idealizations are incorporated merely for convenience, in allowing clear identification of physical interactions within the coreflow, at low (axial) Mach numbers; sharp pressure and temperature variation are obviously precluded. These simplifying assumptions are in no way essential to the solution; variable viscosity, thermal conductivity, etc., can be radily incorporated in the numerical solution algorithm.

The dimensionless equations of motion are as follows, for the region

$$0 < x < 1, \quad 0 < r < 1, \quad t > 0:$$

CONTINUITY:

$$\frac{\partial \rho}{\partial t} + \frac{1}{r}\frac{\partial}{\partial r}(r\rho v) + \frac{\partial \rho u}{\partial x} = S_1 = 0 \tag{2.9}$$

RADIAL MOMENTUM:

$$\frac{\partial \rho v}{\partial t} + \frac{1}{r}\frac{\partial}{\partial r}(r\rho v^2) + \frac{\partial \rho v u}{\partial x} = S_2 \tag{2.10}$$

AXIAL MOMENTUM:

$$\frac{\partial \rho u}{\partial t} + \frac{1}{r}\frac{\partial}{\partial r}(r\rho u v) + \frac{\partial}{\partial x}\left(\rho u^2 + \frac{p}{\gamma M_o^2}\right) = S_3 \tag{2.11}$$

THERMAL ENTHALPY:

$$\frac{\partial \rho h}{\partial t} + \frac{1}{r}\frac{\partial}{\partial r}(\gamma r \cdot \rho h v) + \frac{\partial}{\partial x}(\gamma \rho h u) = S_4 \tag{2.12}$$

where the right-hand side (source) terms are defined:

$$S_2 \equiv \frac{4/3}{R_{eo}} \frac{1}{r}\left(\frac{\partial v}{\partial r} - \frac{v}{r}\right) + \frac{1}{R_{eo}}\left(\frac{\partial^2 v}{\partial x^2} + \frac{1}{3}\frac{\partial^2 u}{\partial r \partial x} + \frac{4}{3}\frac{\partial^2 v}{\partial r^2}\right) - \frac{\partial p}{\partial r} / \gamma M_o^2 \tag{2.13}$$

$$S_3 \equiv \frac{1/r}{R_{eo}}\left(\frac{\partial u}{\partial r} + \frac{1}{3}\frac{\partial v}{\partial r}\right) + \frac{1}{R_{eo}}\left(\frac{\partial^2 u}{\partial r^2} + \frac{4}{3}\frac{\partial^2 u}{\partial x^2} + \frac{\partial^2 v}{\partial r \partial x}\right) \tag{2.14}$$

$$S_4 \equiv \gamma\left(v\frac{\partial p}{\partial r} + u\frac{\partial p}{\partial x}\right) + \frac{\gamma/P_r}{R_{eo}}\left(\frac{1}{r}\frac{\partial h}{\partial r} + \frac{\partial^2 h}{\partial r^2} + \frac{\partial^2 h}{\partial x^2}\right) + \frac{M_o^2}{R_{eo}}\gamma(\gamma-1)\left\{\frac{4}{3}\left[\frac{\partial^2 u}{\partial x^2} + \left(\frac{\partial v}{\partial r}\right)^2 + \left(\frac{v}{r}\right)^2\right] + \left(\frac{\partial u}{\partial r}\right)^2 + \left(\frac{\partial v}{\partial x}\right)^2 - 4\left[\frac{v}{r}\left(\frac{\partial v}{\partial r} + \frac{\partial u}{\partial x}\right) + \frac{\partial v}{\partial r}\frac{\partial u}{\partial x}\right]\right\}. \tag{2.15}$$

The parameters, γ, Pr, M_o^2, R_{eo} are all constants.

The differential system for the coreflow can be written in short notation,

$$\frac{\partial U_k}{\partial t} + \frac{1}{r}\frac{\partial}{\partial r}(r F_k) + \frac{\partial G_k}{\partial x} = S_k, \quad k = 1, \cdots 4 \tag{2.16}$$

where U_k is the non-primitive dependent variable vector, with the components defined:

$$U_1 = \rho, \quad U_2 = \rho v, \quad U_3 = \rho u, \quad U_4 = \rho h \tag{2.17}$$

while the flux terms $F_k(U)$, $G_k(U)$ depend only upon the vector U (when , M_o are considered as constant parameters:

$$F_1 = \rho v, \quad F_2 = \rho v^2, \quad F_3 = \rho u v, \quad F_4 = \gamma \rho h v \tag{2.18}$$

$$G_1 = \rho u, \quad G_2 = \rho v u, \quad G_3 = \rho u^2 + p/\gamma M_o^2, \quad G_4 = \gamma \rho h u \tag{2.19}$$

Note that incorporation of the pressure gradient within the S_2 source term in the radial momentum equation, while the axial pressure gradient is included within the axial flux comonent, G_3, is merely for convenience in the solution process. In the meantime, the viscous and thermal dissipative terms, $\tilde{}O(1/Reo)$, are expected to be very small over most of the coreflow domain, excluding the neighborhood of the walls.

The Boundary Conditions: The following physical boundary data are available, for the cold-flow simulation:

(a) On the centerline, (t, r=0, x):

$$v = 0; \qquad \partial u/\partial r = \partial \rho/\partial r = \partial h/\partial r = 0 \tag{2.20}$$

(b) At the porous (injected) surface, (t, r=1, x):

$$v = -v_o(x,t), \qquad u=0, \qquad h = h_o(x,t) \tag{2.21}$$

(c) At the (nonpermeable solid) head-end closure, (t, r, x=0):

$$v = 0, \quad u = 0, \quad h = h_H(r,t) \tag{2.22}$$

The functions $v_o(x,t)$, $h_o(x,t)$ and $h_H(r,t)$ are arbitrary imposed (generally variable) distributions.

(d) The exit plane, defined by (t, r, x=L), forms an entrance into a short, convergent nozzle section. This nozzle section is treated separately from the rest of the flow field; several assumptions are incorporated, as follows:

(d.1) The throat, $A_t(t)$, is variable but remains sonic at all times.

(d.2) The convergent section is short, and introduces no dynamic effect; it responds instantly to any changes, and is considered (in this sense) quasi steady.

(d.3) The sonic surface at the throat is reasonably approximated by a plane encompassing the entire (circular) throat area. In other words, within each computational cell, the flow can be considered quasi one-dimensional.

The last assumption is used to facilitate calculation of the implicit functional relationship

$$f[\,(u/a)^2,\ At/A,\ \ldots] = 0 \tag{2.23}$$

within each computational cell in the discretized flowfield within the nozzle.

The foregoing discussion has summarized the corelflow analytical model, including the equations of motion and the relevant boundary data.

Simulation of the nonsteady flow field, which arises due to perturbation of the exit nozzle can be performed, with the initial data corresponding to steady state. As mentioned earlier, solutions are generated numerically, by a finite-difference algorithm. Prior to the description of the numerical algorithm, two special regions in the flow are discussed in detail: the head-end and the sidewall layer, which appear in the following two sections.

2.2 THE HEAD-END CLOSURE LAYER

A solid, planar head-end closure is considered at x=0, as shown in Fig. 2. The flow in this region is radially injected inward (from the porous cylindrical wall), then, near the centerline, tends to turn toward the axial direction.

A boundary layer is formed near x=0, to connect the regular flow regime (with apperciable radial and axial motions), with the end-wall where no-slip conditions prevail, viz., v=u=0. Within this layer viscous forces are of importance. The dimensionless parameter

$$0 < \varepsilon \equiv 1/\sqrt{R_{eo}} << 1 \qquad (2.24)$$

can serve as a proper small perturbation quantity. The layer axial coordinate is therefore stretched,

$$y_1 = x/\varepsilon \qquad (2.25)$$

Thus, the independent variable system is transformed from (x, r, t) to (y_1, r, t) in the layer. Further, the dependent variables are now perturbed, as

$$\rho = \rho_0 + \varepsilon\rho_1 \ , \quad v = v_0 + \varepsilon v_1 \ , \quad u = u_0 + \varepsilon u_1 \ , \qquad (2.26)$$
$$h = h_0 + \varepsilon h_1$$

where the dependent variables are

$v_0(y_1,r,t)$, $v_1(y_1,r,t)$, $u_1(y_1,r,t)$ ... etc., all assumed to be of order unity. For convenience, the following abbreviated definitions are introduced:

$$F_0 = \rho_0 v_0 \ , \quad G_0 = \rho_0 u_0 \ , \quad F_1 \equiv \rho_0 v_1 + \rho_1 v_0 \ , \quad G_1 \equiv \rho_0 u_1 + \rho_1 u_0 \qquad (2.27)$$

The transformed axial derivatives are now,

$$\partial/\partial x = \frac{1}{\varepsilon}\partial/\partial y_1 \ , \qquad \partial^2/\partial x^2 = \frac{1}{\varepsilon^2}\partial^2/\partial y_1^2 \qquad (2.28)$$

while the (r,t) variations remain equal to their counterparts in the original equations of motion.

In the remainder of this section we will derive the perturbed system of equations of motion for the layer, and collect hierarchies of equal power of ε.

Obviously, the injection Mach number appears as an additional parameter in the formulation (equations of momentum and energy). In the flow fields of interest for simulation herein, M_o is also very small; in consideration of typical experiments at CSD/UTC with air injection, we find

$$M_o^2 \sim O(1/R_{eo}) \sim \varepsilon^2 \tag{2.29}$$

which adequately represents a range of cold-flow conditions. This offers great simplification in the analysis, although at the cost of narrower range of general application (considering the relative freedom of the two major flow parameters, R_{eo} and M_o).

Therefore a parameter is introduced,

$$K_m \equiv \frac{1/R_{eo}}{\gamma M_o^2} = \frac{\varepsilon^2}{\gamma M_o^2} \sim O(1) \tag{2.30}$$

according to the foregoing considerations.

The question of timescale is not trivial, since it depends upon the range of frequencies of interest. The following reasoning will demonstrate that for the range of conditions considered for the present simulation, the timescale can remain the same one as in the coreflow. The viscous layer thickness is

$$\delta_v \sim R_o/\sqrt{R_{eo}} \tag{2.31}$$

where

$$R_{eo} = v_o^* R_o^* / \nu^* \tag{2.32}$$

The Stokes Layer thickness (for acoustic perturbations with a frequency f_o^*)

$$\delta_{STO} \sim \sqrt{\nu^*/f_o^*} \tag{2.33}$$

The ratio of these two thickness scales is,

$$\delta_v/\delta_{STO} \sim \sqrt{f_o^* R_o^* / \nu^*} = S_{RO}^{1/2} \tag{2.34}$$

where S_{RO} is the relevant (injection) Strouhal number. The range of Strouhal numbers considered is $S_{RO} \sim O(1)$, so one need not introduce any additional timescales.

The continuity equation becomes, after using the perturbed variables, Eqs. (2.26)-(2.28):

$$\frac{\partial}{\partial t}(\rho_o + \varepsilon\rho_1) + \frac{\partial}{\partial r}(\rho_o v_o + \varepsilon F_1) + \frac{1}{\varepsilon}\frac{\partial}{\partial y_1}(\rho_o u_o + \varepsilon G_1 + \varepsilon^2 \rho_1 u_1) = -\frac{1}{r}(F_o + \varepsilon F_1). \tag{2.35}$$

From which the following hierarchy is collected:

ORDER $1/\varepsilon$:

$$\partial G_0/\partial y_1 = 0 \tag{2.36}$$

$$G_o = G_o\ (r,t) \tag{2.37}$$

ORDER ε^0 (ZEROTH):

$$\frac{\partial \rho_0}{\partial t} + \frac{\partial F_0}{\partial r} + \frac{\partial G_1}{\partial y_1} = -\frac{F_0}{r} \tag{2.38}$$

ORDER ε^1 (FIRST):

$$\frac{\partial \rho_1}{\partial t} + \frac{\partial F_1}{\partial r} + \frac{\partial \rho_1 u_1}{\partial y_1} = -\frac{F_1}{r} \tag{2.39}$$

Similarly, the radial momentum equation yields

$$\frac{\partial}{\partial t}\left[F_0 + \varepsilon F_1\right] + \frac{\partial}{\partial r}\left[F_0 V_0 + \varepsilon\left(F_1 V_0 + F_0 V_1\right) + \frac{K_m}{\varepsilon^2}\left(P_0 + \varepsilon P_1 + \varepsilon^2 P_2\right)\right]$$

$$+ \frac{1}{\varepsilon}\frac{\partial}{\partial y_1}\left[F_0 u_0 + \varepsilon\left(F_1 u_0 + F_0 u_1\right)\right] = -\frac{F_0 V_0}{r} - \varepsilon\frac{V_0 F_1 + V_1 F_0}{r}$$

$$+ \frac{4}{3}\cdot O(\varepsilon^2) + \frac{1}{3}\varepsilon\left(\frac{\partial^2 u_0}{\partial r \partial y_1} + \varepsilon\frac{\partial^2 u_1}{\partial r \partial y_1}\right) +$$

$$+ \frac{\partial^2 V_0}{\partial y_1^2} + \varepsilon\frac{\partial^2 V_1}{\partial y_1^2} \tag{2.40}$$

The following hierarchy evolves:

ORDER $1/\varepsilon^2$:

$$\partial P_0/\partial r = 0 \tag{2.41}$$

ORDER $1/\varepsilon$:

$$\partial(F_0 u_0)/\partial y_1 + K_m \partial P_1/\partial r = 0 \tag{2.42}$$

ORDER ε^0 (ZEROTH):

$$\frac{\partial F_0}{\partial t} + \frac{\partial}{\partial r}(F_0 V_0) + \frac{\partial}{\partial y_1}(u_0 F_1 + u_1 F_0) = -\frac{F_0 V_0}{r} + \frac{\partial^2 V_0}{\partial y_1^2} \tag{2.43}$$

ORDER ε^1 (FIRST):

$$\frac{\partial F_1}{\partial t} + \frac{\partial}{\partial r}(V_0 F_1 + V_1 F_0) + \frac{\partial}{\partial y_1}(F_1 u_1) = -(V_0 F_1 + V_1 F_0)/r + \frac{1}{3}\frac{\partial^2 u_0}{\partial r \partial y_1} + \frac{\partial^2 V_1}{\partial y_1^2} . \tag{2.44}$$

The axial momentum yields, after similar treatment:

ORDER $1/\varepsilon^3$:
$$\partial P_0/\partial y_1 = 0 \tag{2.45}$$

ORDER $1/\varepsilon^2$:
$$\partial P_1/\partial y_1 = 0 \tag{2.46}$$

ORDER $1/\varepsilon$:
$$\partial(G_0 u_0)/\partial y_1 = 0 \tag{2.47}$$

Thus, in view of Eq. (2.37):

$$u_0 = u_0 (r,t) \tag{2.48}$$

ORDER ε^0 ZEROTH:

$$\frac{\partial G_0}{\partial t} + \frac{\partial G_0 V_0}{\partial r} + \frac{\partial}{\partial y_1}(u_0 G_1 + u_1 G_0) = -\frac{G_0 V_0}{r} + \frac{4}{3}\frac{\partial^2 u_0}{\partial y_1^2} \tag{2.49}$$

ORDER ε^1 (FIRST):

$$\frac{\partial G_1}{\partial t} + \frac{\partial}{\partial r}(V_0 G_1 + V_1 G_0) + \frac{\partial}{\partial y_1}(u_1 G_1) = -(G_1 V_0 + G_0 V_1)/r + \frac{4}{3}\frac{\partial^2 u_1}{\partial y_1^2} + \frac{1}{3}\frac{\partial^2 V_0}{\partial r \partial y_1} . \tag{2.50}$$

At this point, the lower-order anlaysis results can be summarized:

$$\partial G_o/\partial y_1 = 0 \rightarrow G_o = G_o(r,t)$$

$$\partial p_o/\partial r = 0 \rightarrow \partial \phi_o/\partial r = 0,$$

where: $$\phi_o \equiv \rho_o h_o . \tag{2.51}$$

$$\frac{\partial G_o v_o}{\partial y_1} + K_m \frac{\partial p_1}{\partial r} = 0 \rightarrow G_o \frac{\partial v_o}{\partial y_1} + K_m \frac{\partial p_1}{\partial r} = 0;$$

$$\frac{\partial p_o}{\partial y} = 0 = \frac{\partial p_1}{\partial y} \quad ; \qquad \frac{\partial u_o G_o}{\partial y_1} = 0 \rightarrow u_o = u_o(r,t)$$

Based on the foregoing, along with the boundary data:

$$u_o \ (y_1 = 0, r, t) = 0 \tag{2.52}$$

the natural choice of solution for u_o is the trivial one,

$$u_o \ (y_1, r, t) = 0 \tag{2.53}$$

Thus, $G_o(y_1, r, t) = 0$. Further, from Eq. (2.42),

$$\partial p_1/\partial r = 0 \tag{2.54}$$

which therefore leaves only time-dependent pressure within the layer, up to $O(\varepsilon^2)$:

$$p_o = p_o(t) \quad , \quad p_1 = p_1(t) \tag{2.55}$$

which implies also, for $\phi = \rho h$:

$$\phi_o = \phi_o(t) \quad , \quad \phi_1 = \phi_1(t) \tag{2.56}$$

With the foregoing results incorporated, the energy equation becomes much simpler to handle; the following hierarchy is obtained:

<u>ORDER ε^0 (ZEROTH)</u>:

$$\frac{\partial \phi_o}{\partial t} + \gamma \phi_o \frac{\partial u_1}{\partial y_1} + \gamma \phi_o \frac{\partial v_o}{\partial r} = -\frac{\gamma \phi_o v_o}{r} + \frac{\gamma}{P_r} \frac{\partial^2 h_o}{\partial y_1^2} \tag{2.57}$$

Note that the specific enthalpy, h_o, and the density may vary with both y_1 and r, despite $\phi_o = \phi_o(t)$.

ORDER ε^1 (FIRST):

$$\frac{\partial\phi_1}{\partial t} + \gamma\phi_1\frac{\partial u_1}{\partial y_1} + \gamma\frac{\partial\phi_1 v_o}{\partial r} + \gamma\phi_o\frac{\partial v_1}{\partial r} = -\gamma(\phi_o v_1 + \phi_1 v_o)/r$$
$$+ \frac{\gamma}{P_r}\partial^2 h_1/\partial y_1^2 \quad . \qquad (2.58)$$

To lowest order in the perturbation quantity, ε, one may collect the following differential system, written in convection form.

$$\frac{\partial\rho_o}{\partial t} + \frac{\partial F_o}{\partial r} + \frac{\partial G_1}{\partial y_1} = -\frac{F_o}{r} \qquad (2.59)$$

$$\rho_o\frac{\partial v_o}{\partial t} + F_o\frac{\partial v_o}{\partial r} + G_1\frac{\partial v_o}{\partial y_1} = \frac{\partial^2 v_o}{\partial y_1^2} \qquad (2.60)$$

$$\rho_o\frac{\partial u_1}{\partial t} + F_o\frac{\partial u_1}{\partial r} + G_1\frac{\partial u_1}{\partial y_1} = \frac{4}{3}\frac{\partial^2 u_1}{\partial y_1^2} + \frac{1}{3}\frac{\partial^2 v_o}{\partial r\partial y_1} \qquad (2.61)$$

$$\rho_o\frac{\partial h_o}{\partial t} + F_o\frac{\partial h_o}{\partial r} + G_1\frac{\partial h_o}{\partial y_1} = \frac{1}{P_r}\frac{\partial^2 h_o}{\partial y_1^2} + \frac{dP_o}{dt} \qquad (2.62)$$

Note that $G_1 = \rho_o u_1$ here. With $p_o(t)$ imposed externally, (as expected), this system forms a closure for ρ_o, h_o, V_o and u_1. The only parameter appearing explicitly is the Prandtl number, which is of order unity.

The associated boundary data are as follows. At $y_1=0$, the head-end plane:

$$v_o\ (0,r,t) - u_1\ (0,r,t) = 0 \qquad (2.63)$$

$$h_o\ (0,r,t) = H_w\ (r,t) \qquad (2.64)$$

where H_w is an arbitrary function. Note that

$$\rho_o(0,r,t) = \frac{\gamma}{\gamma-1}\,p_o(t)/H_w(r,t) \qquad (2.65)$$

which follows from the equation of state, with $p_o(t)$ impressed upon the layer by the outer - flow field. Now in the radial direction, the boundary data are as follows. At the injected porous wall, r=1:

$$v_o(y_1,1,t) = -V_w \tag{2.66}$$

$$u_1(y_1,1,t) = 0 \tag{2.67}$$

$$h_o(y_1,1,t) = H_w(t) \tag{2.68}$$

On the centerline, r=0:

$$v_o(y_1,0,t) = 0 \tag{2.69}$$

$$\partial u_1/\partial r\ (y_1,0,t) = 0 \tag{2.70}$$

$$\partial h_o/\partial r\ (y_1,0,t) = 0 \tag{2.71}$$

Evidently, the second-order derivatives in Eqs. (2.60) through (2.62) are in the axial direction (y_1), so that the velocities and thermal enthalphy must match their outer-field counterparts at an intermediate region of common validity.

In summary, the two important results of lower-order analysis herein are as follows.

(1) Pressure is uniform within the layer up to $O(\varepsilon^2)$ - at least, i.e.,

$$p_o = p_o(t), \qquad p_1 = p_1(t)$$

which can be expected, in view of the thin layer assumption as well as the low velocities.

(2) The axial velocity is small and of order ε, namely,

$$u_o(y_1,r,t) = 0$$

while $u_1 \neq 0$ in general.

The zeroth-order differential system, Eqs. (2.59)-(2.62), with the boundary data, Eqs. (2.63)-(2.71), form a closure. Obviously, the pressure $p_o(t)$ is impressed upon the layer externally. Also, external boundary data is required for solution for the two momentum equations and the enthalpy equation, as expected; this would enter through inner-outer matching. The actual method of solution will not be discussed herein.

2.3 THE INJECTED SIDEWALL LAYER

2.3.0 THE SINGULAR PERTURBATION SYSTEM

A porous, injected cylindrical pipe is considered, as shown in Fig. 3. The flow region of interset is close to the surface, where viscous forces are expected to be appreciable within a thin layer.

For the neighborhood of r=1, the following transform is proposed for the radial coordinate:

$$y = (1-r)/\varepsilon \tag{2.72}$$

which magnifies the wall layer, with

$$0 < \varepsilon \equiv 1/\sqrt{R_{eo}} << 1 \tag{2.73}$$

as defined earlier, in Eq. (2.24). Thus,

$$\partial/\partial r = -\frac{1}{\varepsilon}\partial/\partial y \tag{2.74a}$$

$$\partial^2/\partial r^2 = \frac{1}{\varepsilon^2}\partial^2/\partial y^2 \tag{2.74b}$$

and

$$r = 1 - \varepsilon y \tag{2.75}$$

Again the assumption for small injection Mach number is constrained by:

$$K_m \equiv \frac{1/R_{eo}}{\gamma M_o^2} = \frac{\varepsilon^2}{\gamma M_o^2} \sim O(1) \tag{2.76}$$

in agreement with the available experimental data.

The independent variables are (x,y,t), while the associated dependent variables, in the wall-layer, are perturbed,

$$\rho = \rho_o + \varepsilon\rho_1 , \qquad V = V_o + \varepsilon V_1 , \qquad u = u_o + \varepsilon u_1$$

$$h = h_o + \varepsilon h_1 \tag{2.77}$$

the following abbreviations are introduced,

$$F_o = \rho_o V_o , \; G_o = \rho_o u_o , \; G_1 \equiv \rho_o u_1 + \rho_1 u_o , \; F_1 \equiv \rho_o V_1 + \rho_1 V_o \tag{2.78}$$

These are not to be confused with their head-end counterparts; although the notation is the same, the functional dependences are quite different, obviously.

For reasons explained fully in the head-end wall layer analysis, no further timescales or (axial) length scales need to be introduced.

2.3.1 DEPRIVATION

For the perturbation variables of Eqs. (2.72)-(2.78), the continuity equation is:

$$\frac{\partial}{\partial t}(\rho_0+\varepsilon\rho_1)-\frac{1}{\varepsilon}\frac{\partial}{\partial y}(F_0+\varepsilon F_1+\varepsilon^2\rho_1 V_1)+\frac{\partial}{\partial x}(G_0+\varepsilon G_1)$$
$$=-(1+\varepsilon y)(F_0+\varepsilon F_1) \tag{2.79}$$

The following hierarchy is collected:

<u>ORDER $1/\varepsilon$</u>

$$-\partial F_0/\partial y=0 \tag{2.80}$$
$$F_0=F_0(x,t) \tag{2.81}$$

<u>ORDER ε^0 (ZEROTH)</u>

$$\frac{\partial\rho_0}{\partial t}+\frac{\partial G_0}{\partial x}-\frac{\partial F_1}{\partial y}=-F_0 \tag{2.82}$$

<u>ORDER ε^1 (FIRST)</u>

$$\frac{\partial\rho_1}{\partial t}+\frac{\partial G_1}{\partial x}-\frac{\partial\rho_1 V_1}{\partial y}=-F_1-yF_0 \tag{2.83}$$

The <u>radial momentum</u> balance becomes:

$$\frac{\partial}{\partial t}(F_0+\varepsilon F_1)+\frac{\partial}{\partial x}\left[F_0u_0+\varepsilon(F_0u_1+F_1u_0)\right]-\frac{1}{\varepsilon}\frac{\partial D_0}{\partial y}$$
$$-\frac{1}{\varepsilon}\frac{\partial}{\partial y}\left[\frac{K_m}{\varepsilon^2}(P_0+\varepsilon P_1)\right]=-(1+\varepsilon y)D_0+D_1\ ,$$

$$D_0\equiv F_0V_0+\varepsilon(F_0V_1+F_1V_0)+\varepsilon^2(F_1+\rho_1V_0)V_1\ ,$$

$\longrightarrow$

$$D_1 \equiv \frac{4}{3}\varepsilon^2(1+\varepsilon y)\left\{\frac{-1}{\varepsilon}\left(\frac{\partial v_0}{\partial y}+\varepsilon\frac{\partial v_1}{\partial y}\right)-(v_0+\varepsilon v_1)(1+\varepsilon y)\right\}$$
$$+\varepsilon^2\left\{\frac{\partial^2 v_0}{\partial x^2}+\varepsilon\frac{\partial^2 v_1}{\partial x^2}-\frac{1}{3}\cdot\frac{1}{\varepsilon}\left(\frac{\partial^2 u_0}{\partial x\partial y}+\varepsilon\frac{\partial^2 u_1}{\partial x\partial y}\right)\right\}$$
$$+\frac{4}{3}\varepsilon^2\left(\frac{1}{\varepsilon^2}\right)\left(\frac{\partial^2 v_0}{\partial y^2}+\varepsilon\frac{\partial^2 v_1}{\partial y^2}\right). \tag{2.84}$$

The hierarchy obtained is:

ORDER $1/\varepsilon^3$:

$$-K_m\,\partial P_0/\partial y = 0 \tag{2.85}$$

Thus, $P_0 = P_0(x,t)$

ORDER $1/\varepsilon^2$:

$$-K_m\,\partial P_1/\partial y = 0 \longrightarrow P_1 = P_1(x,t) \tag{2.86}$$

ORDER $1/\varepsilon$:

$$-\partial F_0 v_0/\partial y = 0 \tag{2.87}$$

ORDER ε^0 (ZEROTH):

$$\frac{\partial F_0}{\partial t}+\frac{\partial F_0 u_0}{\partial x}-\frac{\partial}{\partial y}\left(F_0 v_1+F_1 v_0\right)=-F_0 v_0+\frac{4}{3}\frac{\partial^2 v_0}{\partial y^2}. \tag{2.88}$$

ORDER ε^1 (FIRST):

$$\frac{\partial F_1}{\partial t}+\frac{\partial}{\partial x}\left(F_0 u_1+F_1 u_0\right)-\frac{\partial}{\partial y}\left[v_1\left(F_1+\rho_1 v_0\right)\right]=-F_0 v_0 y$$
$$-\left(F_0 v_1+F_1 v_0\right)+\frac{4}{3}\frac{\partial^2 v_1}{\partial y^2}+\frac{4}{3}\frac{\partial v_0}{\partial y}-\frac{1}{3}\frac{\partial^2 u_0}{\partial x\partial y}. \tag{2.89}$$

The axial momentum balance is:

$$\frac{\partial}{\partial t}(G_0+\varepsilon G_1)+\frac{\partial}{\partial x}\left[G_0u_0+\varepsilon(G_1u_0+G_0u_1)\right]+\frac{K_m}{\varepsilon^2}\frac{\partial}{\partial x}(P_0+\varepsilon P_1)$$

$$-\frac{1}{\varepsilon}\frac{\partial D_2}{\partial y}=-(1+\varepsilon y)D_2+\varepsilon^2(1+\varepsilon y)\left(\frac{-1}{\varepsilon}\right)\left(\frac{\partial u_0}{\partial y}+\varepsilon\frac{\partial u_1}{\partial y}\right)$$

$$+\frac{\varepsilon^2}{3}(1+\varepsilon y)\left(-\frac{1}{\varepsilon}\right)\left(\frac{\partial v_0}{\partial y}+\varepsilon\frac{\partial v_1}{\partial y}\right)+\frac{\partial^2 u_0}{\partial y^2}+\varepsilon\frac{\partial^2 u_1}{\partial y^2}+\frac{4}{3}\varepsilon^2\frac{\partial^2 u_0}{\partial x^2}$$

$$+\varepsilon^2\frac{1}{3}\left(-\frac{1}{\varepsilon}\right)\frac{\partial^2}{\partial x\partial y}(v_0+\varepsilon v_1);$$

$$D_2\equiv G_0v_0+\varepsilon(G_0v_1+G_1v_0)+\varepsilon^2(G_1v_1+\rho_1u_1v_0). \quad (2.90)$$

The associated hierarchy is:

ORDER $1/\varepsilon^3$:

$$K_m\partial P_0/\partial x=0 \quad (2.91)$$

hence, ... $P_0=P_0(t)$ (2.92)

ORDER $1/\varepsilon$:

$$K_m\frac{\partial P_1}{\partial x}-\frac{\partial}{\partial y}(F_0u_0)=0 \quad (2.93)$$

where we used $F_0u_0 = G_0v_0$. This equation is of great importance, as will be shown later.

ORDER ε^0 (ZEROTH):

$$\frac{\partial G_0}{\partial t}+\frac{\partial G_0u_0}{\partial x}-\frac{\partial}{\partial y}(G_0v_1+G_1v_0)=-G_0v_0+\frac{\partial^2 u_0}{\partial y^2}. \quad (2.94)$$

ORDER ε^1 (FIRST):

$$\frac{\partial G_1}{\partial t}+\frac{\partial}{\partial x}(G_1u_0+G_0u_1)-\frac{\partial}{\partial y}(G_1v_1+\rho_1v_0u_1)=$$

$$=-(G_1v_0+G_0v_1)-G_0v_0y+\frac{\partial^2 u_1}{\partial y^2}+\frac{\partial u_0}{\partial y}-\frac{1}{3}\frac{\partial v_0}{\partial y}$$

$$-\frac{1}{3}\frac{\partial^2 v_0}{\partial x\partial y} \quad (2.95)$$

After similar substitution, the enthalpy equation in the wall layer yields the following hierarchy, for

$$\Phi_0 \equiv \rho_0 h_0 \ , \qquad \Phi_1 \equiv \rho_0 h_1 + \rho_1 h_0 \ . \tag{2.96}$$

ORDER $1/\varepsilon$

$$-\gamma \frac{\partial \Phi_0 V_0}{\partial y} = - V_0 \frac{\partial \Phi_0}{\partial y} \tag{2.97}$$

Note that on the left hand side, according to Eqs. (2.80), (2.87)

$$\partial V_0 / \partial y = 0$$

(since $F_0 \neq 0$ in general). Now, according to Eq. (2.92), $p_0 = p_0(t)$, so that both sides are identically zero, as

$$\Phi_0 = \gamma P_0(t)/(\gamma - 1) = \Phi_0(t) \ .$$

Therefore, Eq. (2.97) does not yield any new information.

ORDER ε^0 (ZEROTH)

$$\frac{\partial \Phi_0}{\partial t} + \frac{\partial}{\partial x}\gamma\Phi_0 u_0 - \frac{\partial}{\partial y}(\gamma\Phi_1 V_0 + \gamma\Phi_0 V_1) = -\gamma\Phi_0 V_0 + \frac{\gamma}{P_r}\frac{\partial^2 h_0}{\partial y^2}$$
$$+ (\gamma - 1)\left[u_0 \frac{\partial \Phi_0}{\partial x} - \left(V_1 \frac{\partial \Phi_0}{\partial y} + V_0 \frac{\partial \Phi_1}{\partial y}\right)\right] . \tag{2.98}$$

ORDER ε^1 (FIRST)

$$\frac{\partial \Phi_1}{\partial t} + \frac{\partial}{\partial x}(\gamma\Phi_1 u_0 + \gamma\Phi_0 u_1) - \frac{\partial}{\partial y}\gamma\Phi_1 V_1 = -\gamma\left\{\Phi_0 V_0 y + \Phi_0 V_1 + \Phi_1 V_0\right\}$$
$$+ (\gamma - 1)\left\{\left(u_1 \frac{\partial \Phi_0}{\partial x} + u_0 \frac{\partial \Phi_1}{\partial x}\right) - V_1 \frac{\partial \Phi_1}{\partial y}\right\} + \frac{\gamma}{P_r}\left(\frac{\partial^2 h_1}{\partial y^2} - \frac{\partial h_0}{\partial y}\right) . \tag{2.99}$$

This concludes the derivation of the perturbed equations of motion.

2.3.2 ANALYSIS-SIDEWALL LAYER

The results of lower-order analysis can be summarized as follows. From Eq. (2.81),

$$\rho_o V_o = F_o(x,t)$$

while from Eq. (2.87), using the last equation,

$$v_o = v_o\ (x,t) \tag{2.100}$$

Thus $_o$, v_o and F_o are all independent of y. Further, from Eqs. (2.85) and (2.91) clearly

$$p_o = p_o(t) \rightarrow \rho_o h_o = \phi_o(t)$$

while from Eq. (2.86),

$$p_1 = p_1(x,t); \tag{2.101}$$

so that both p_o and p_1 are independent of y, but $p_o(t)$ is uniform within the entire chamber, as expected. As a consequence of Eq. (2.101),

$$\rho_o h_1 + \rho_1 h_o = \phi_1(x,t) \tag{2.102}$$

One may now proceed to solve Eq. (2.93) directly for u_o:

$$F_o\, \partial u_o/\partial y = K_m\, \partial p_1/\partial x$$

$$u_o(x,y,t) = \left(\frac{K_m}{F_o}\frac{\partial p_1}{\partial x}\right) y \tag{2.103}$$

with the boundary condition, (no-slip):

$$u_o\ (x,0,t) = 0 \tag{2.104}$$

Of course, the (x,t) dependence of u_o still remains to be found. However, its dependence upon the layer coordinate, y, is found to be linear; this result is certainly not obvious, and has several important implications.

The shear stress within the layer,

$$-\tau^{\circ}_{xy} \sim \partial u_o/\partial y = K_m\left(\frac{\partial p_1}{\partial x}\right)/F_o \tag{2.105}$$

is obviously nonzero in general, while the associated azymuthal vorticity within the layer is independent of distance from the wall at any given station (x,t). Even more striking is the vanishing of the viscous dissipation term at zeroth order:

$$\partial^2 u_0/\partial y^2 = 0 \tag{2.106}$$

which leaves in the zeroth-order axial momentum equation a balance of inertial terms, strictly, ct. Eq. (2.94). This explains physically the success (up to first order) of modeling this family of injected flows by assuming rotational, inviscid motions; such modeling indeed obtains solutions for the axial velocity profile, which satisfy the no-slip condition at the wall (r=1).

It further appears that the shear stress, Eq. (2.105), is proportional to the first-order axial pressure gradient, while being inversely proportional to the injected mass flux, as would be expected. Of course, $\partial P_1/\partial x$ depends on F_0, and one expects their ratio to be finite at the limit as zero injection is approached.

In addition to the foregoing result for axial velocity, the zeroth order formulation can be utilized to solve for the y-dependence of the other dependent variables. The continuity equation can be written now as

$$\frac{\partial \rho_0}{\partial t} + \frac{\partial}{\partial x}\rho_0 u_0 - \frac{\partial F_1}{\partial y} + F_0 = 0$$

From Eqs. (2.81) and (2.100) we know that F_0 and ρ_0 are independent of y. Hence, one may split the foregoing equation,

$$\partial \rho_0/\partial t + F_0(x,t) = C_0(x,t) \tag{2.107}$$

$$\frac{\partial}{\partial x}\left(\frac{K_m}{V_0}\frac{\partial P_1}{\partial x}\right)y - \frac{\partial F_1}{\partial y} = -C_0(x,t) \tag{2.108}$$

where $C_0(x,t)$ is a common separation parmeter, with a range of values fully determined by the boundary data.

The second equation yields

$$F_1(y,x,t) = B_0(x,t) + C_0(x,t)\cdot y + \frac{\partial g_0}{\partial x}y^2/2 \tag{2.109}$$

where:

$$B_0(x,t) = F_1(0,x,t) \tag{2.110}$$

$$g_0(x,t) \equiv \frac{K_m}{V_0}\frac{\partial P_1}{\partial x} \tag{2.111}$$

Similarly, the zeroth order radial momentum equation is split:

$$\partial F_0/\partial t + F_0 V_0 = C_1(x,t) \qquad (2.112)$$

$$\frac{\partial}{\partial x}\left(K_m \frac{\partial P_1}{\partial x}\right) y - \frac{\partial}{\partial y}\left(V_0 F_1 + V_1 F_0\right) = -C_1(x,t) \qquad (2.113)$$

The last equation can be integrated,

$$V_1(y,x,t) = B_1(x,t) + \frac{C_1 - V_0 C_0}{F_0} y + \frac{K_m}{F_0}\frac{\partial P_1}{\partial x} \cdot \frac{\partial \ln V_0}{\partial x} \cdot \frac{y^2}{2},$$

$$B_1(x,t) = V_1(0,x,t) \qquad (2.114)$$

The foregoing results for F_1 and v_1 yield for the first-order density:

$$\rho_1(y,x,t) = (F_1 - \rho_0 V_1)/V_0 = (B_0 - \rho_0 B_1)/V_0 +$$

$$+ (2C_0 - C_1/V_0) y + \frac{K_m}{2V_0^2}\left[\frac{\partial^2 P_1}{\partial x^2} - 2\frac{\partial P_1}{\partial x} \cdot \frac{1}{V_0}\frac{\partial V_0}{\partial x}\right] y^2 \qquad (2.115)$$

Note that: $\rho_1(0,x,t) = (B_0 - \rho_0 B_1) v_0$

so that ρ_1 is uniquely defined and an additional integration constant is not necessary. Also, according to Eqs. (2.107) and (2.112),

$$\rho_0 \partial V_0/\partial t = C_1 - C_0 V_0 \qquad (2.116)$$

Now, since $\phi_1 \equiv \rho_1 h_0 + \rho_0 h_1$, and we already found that

$$\partial\phi_1/\partial y = \partial h_0/\partial y = \partial\rho_0/\partial y = 0$$

then:

$$h_1(y,x,t) = -\frac{h_0}{\rho_0}\rho_1(y,x,t) + B_2(x,t) \qquad (2.117)$$

Thus, $h_1(y,x,t)$ is second order in y, like ρ_1; the appropriate boundary condition is,

$$B_2(x,t) = h_1(0,x,t) - h_o(B_o - \rho_o B_1)/F_o \qquad (2.118)$$

For the axial momentum, after dividing through by $F_o u_o$, Eq. (2.94) leads to:

$$\frac{1}{F_o}\frac{\partial \rho_o}{\partial t} + 1 + \frac{1}{V_o}\frac{\partial \ln u_o}{\partial t} + \frac{u_o}{F_o}\frac{\partial \rho_o}{\partial x} + \frac{2}{V_o}\frac{\partial u_o}{\partial x} -$$

$$-\frac{1}{u_o}\frac{\partial u_1}{\partial y} - \frac{1}{F_o}\frac{\partial F_1}{\partial y} - \frac{F_1}{F_o}\frac{\partial \ln u_o}{\partial y} = 0 .$$

(2.119)

Now, according to the foregoing results:

$$\frac{1}{F_o}\frac{\partial \rho_o}{\partial t} + 1 = C_o/F_o \qquad (2.120a)$$

$$-\frac{1}{F_o}\frac{\partial F_1}{\partial y} = -\frac{1}{F_o}(\partial g_o/\partial x)y - C_o/F_o \qquad (2.120b)$$

$$-\frac{F_1}{F_o}\partial \ln u_o/\partial y = -F_1/F_o y \qquad (2.120c)$$

Substitution into Eq. (2.119) yields, after some manipulation:

$$\frac{\partial u_1}{\partial y} = \left[\rho_o\frac{\partial U_o}{\partial x} - \frac{1}{2}\frac{\partial}{\partial x}(\rho_o U_o)\right]U_o y^2/F_o +$$

$$\left(\frac{1}{V_o}\frac{\partial U_o}{\partial t} - \frac{C_o U_o}{F_o}\right)y - B_o U_o/F_o .$$

(2.121)

where

$$U_o(x,t) \equiv \frac{K_m}{F_o}\frac{\partial p_1}{\partial x} = g_o/\rho_o = u_o/y . \qquad (2.122)$$

thus,

$$u_1(y,x,t) = \frac{U_o}{F_o}\left[\rho_o\frac{\partial U_o}{\partial x} - \frac{1}{2}\frac{\partial}{\partial x}(\rho_o U_o)\right]y^3/3 +$$

$$+\left(\frac{1}{V_o}\frac{\partial U_o}{\partial t} - \frac{C_o U_o}{F_o}\right)y^2/2 - B_o U_o y/F_o \qquad (2.123)$$

and

$$u_1(0,x,t) = 0$$

satisfying the no-slip condition at the wall. Thus, the perturbed axial velocity is third order in its y-dependence, and the corresponding viscous dissipation term (unlike its zeroth-order counterpart), does not vanish.

The zeroth order energy equation can now be written as

$$-\frac{\partial \phi_0}{\partial t}\Big/\gamma\phi_0 = \frac{\partial u_0}{\partial x} - \frac{\partial v_1}{\partial y} + V_0 \tag{2.124}$$

Now

$$\partial u_0/\partial x = y\,\partial U_0/\partial x$$

and

$$\partial v_1/\partial y = \frac{C_1 - V_0 C_0}{F_0} + U_0 \frac{\partial \ln V_0}{\partial x}\cdot y$$

Hence, the right-hand side of Eq. (2.124) becomes, after substitution,

$$\frac{\partial u_0}{\partial x} - \frac{\partial v_1}{\partial y} + V_0 = \left(V_0 - \frac{C_1 - V_0 C_0}{F_0}\right) + y\left[\frac{\partial U_0}{\partial x} - U_0 \frac{\partial \ln V_0}{\partial x}\right] \tag{2.125}$$

Now the left hand side of Eq. (124) depends only on t; it therefore remains that the term in square brackets formally vanish. Thus,

$$\frac{\partial U_0}{\partial x} - U_0 \frac{\partial \ln V_0}{\partial x} = 0$$

$$\therefore \quad U_0/V_0 = C_4(t), \qquad V_0 \neq 0 \tag{2.126}$$

One may turn now to the first-order energy equation, which seems to yield some simple and highly useful rseults even without full solution. Equation (2.99), written in terms of pressure, reads:

$$\frac{\partial p_1}{\partial t} + \gamma \frac{\partial}{\partial x}(p_1 u_0 + p_0 u_1) - \gamma \frac{\partial}{\partial y} p_1 v_1 = -\gamma\left[p_0 V_0 y + (p_1 V_0 + p_0 V_1)\right]$$
$$+ (\gamma - 1)\left[u_1 \cancel{\frac{\partial p_0}{\partial x}} + u_0 \frac{\partial p_1}{\partial x} - \cancel{v_1 \frac{\partial p_1}{\partial y}}\right]$$
$$+ \frac{\gamma}{Pr}\left(\frac{\gamma - 1}{\gamma}\right)\left[-\cancel{\frac{\partial h_0}{\partial y}} + \frac{\partial^2 h_1}{\partial y^2}\right]$$

(2.127)

After some manipulation one obtains:

$$\frac{\partial p_1}{\partial t} + \gamma p_1\left(\frac{\partial u_0}{\partial x} - \frac{\partial v_1}{\partial y} + v_0\right) + \gamma p_0\left(\frac{\partial u_1}{\partial x} + v_0 y + v_1\right)$$
$$+ u_0 \partial p_1/\partial x - \frac{\gamma-1}{P_r} \partial^2 h_1/\partial y^2 = 0 \tag{2.128}$$

The first bracketed term, after using Eqs. (2.125) and (2.126), is simply

$$v_0 - (C_1 - v_0 C_0)/F_0$$

The enthalpy term, according to Eqs. (2.115) and (2.117) is:

$$\frac{\partial^2 h_1}{\partial y^2} = \frac{h_0}{V_0}\left(\frac{\partial^2 p_1}{\partial x^2} - 2\frac{\partial p_1}{\partial x}\cdot\frac{1}{V_0}\frac{\partial V_0}{\partial x}\right)\frac{K_m}{F_0} = h_0\frac{\partial}{\partial x}\left(g_0/V_0\right). \tag{2.129}$$

The axial velocity gradient is, from Eq. (2.123):

$$\partial u_1/\partial x = \frac{\partial}{\partial x}\left[\frac{U_0}{V_0}\frac{\partial U_0}{\partial x} - \frac{V_0}{F_0}\cdot\frac{1}{2}\frac{\partial}{\partial x}\rho_0 U_0\right] y^3/3 +$$
$$+ \frac{\partial}{\partial x}\left[\frac{1}{V_0}\frac{\partial U_0}{\partial t} - \frac{C_0 U_0}{F_0}\right] y^2/2 - \frac{\partial}{\partial x}\left[\frac{B_0 U_0}{F_0}\right] y \tag{2.130}$$

Substitution of the last results along with the appropriate expression for v_1, into Eq. (2.128) and collection of equal powers of y yields:

$$\gamma p_0\left\{\frac{1}{\gamma p_0}\frac{\partial p_1}{\partial t} + \frac{p_1}{p_0}\left(v_0 - \frac{C_1 - V_0 C_0}{F_0}\right) - \frac{1/P_r}{\rho_0}\frac{\partial}{\partial x}\left(\frac{\rho_0 U_0}{V_0}\right) + B_1\right\} +$$
$$+ \gamma p_0\left\{-\frac{\partial}{\partial x}\left(\frac{B_0 U_0}{F_0}\right) + v_0 + \frac{C_1 - V_0 C_0}{F_0} + \frac{U_0}{\gamma p_0}\frac{\partial p_1}{\partial x}\right\} y +$$
$$+ \gamma p_0\left\{\frac{U_0}{V_0}\frac{\partial V_0}{\partial x} + \frac{\partial}{\partial x}\left(\frac{1}{V_0}\frac{\partial U_0}{\partial t} - \frac{C_0 U_0}{F_0}\right)\right\} y^2/2 +$$
$$+ \frac{\partial}{\partial x}\left\{\frac{U_0}{V_0}\cdot\frac{\rho_0}{2}\cdot\frac{\partial}{\partial x}\left(\frac{U_0}{\rho_0}\right)\right\} y^3/3 = 0 \tag{2.131}$$

Compatibility with the foregoing derivation (in which y and (x,t) variable separation was implemented), can be maintained, provided each of the bracketed terms in Eq. (2.131) vanishes identically. The resulting four compatibility relations (partial differential) would determine the behavior of the wall sublayer system up to the first order in ε, the small perturbation quantity. However, a total of four undetermined coefficients (at most) should arise necessarily, to accommodate coupling with the outer, inviscid (core) flowfield.

Of particular interest in the present analysis is the pressure,

$$p(y,x,t) \doteq p_o(t) + \varepsilon p_1(x,t)$$

which is a directly measurable quantity. From the axial momentum balance in perturbed form, cf. Eq. (2.90), it is evident that the rotational ("inviscid") coreflow can not sustain a first order term like $\partial p_1/\partial x$ herein; the lowest-order axial pressure gradient effect evolves only at second order, or $\varepsilon^2 p_2$ level. This is clearly borne out in the analyses of Culick, and others, in which the axial pressure drop is proportional to M_o^2 (Mach number of injection, squared), or to ε^2 according to the convention employed here, cf. Eq. (2.76).

This, however, is not what is observed in the recent injected cold flow experiments of Brown, et al at CSD/UTC; the measured axial pressure profiles clearly indicate variation of order $M_o \sim \varepsilon$, or first order.

It therefore seems that the viscous wall layer, with its inherent first-order dissipative processes, impresses this axial pressure variation, at first order, over the entire cross section of the injected channel.

To resolve the axial variation of p_1 by the wall layer formulation, the second compatibility condition in Eq. (2.131) can be used, corresponding to the y-term:

$$\frac{\partial}{\partial x}\left(\frac{\overline{B_o} U_o}{F_o}\right) + V_o + \frac{C_1 - V_o C_o}{F_o} + \frac{U_o}{\partial p_o}\frac{\partial p_1}{\partial x} = 0 \tag{2.132}$$

For the special case of uniform (zeroth order) injection at steady state, the presence of a nonzero first-order pressure perturbation would imply physically a corresponding nonzero perturbation upon the mass flux injected, i.e.,

$$B_o = F_1(0,x,t) \neq 0$$

as given by Eq. (2.110). Now at steady state, although B_o is expected to vary with p_1, we have assumed for simplicity that $B_o(x) = \overline{B}_o$ = const.

With the foregoing steady state assumptions, Eq. (2.132) is, for all practical purposes, an ordinary differential equation, for $0<x<L$:

$$\frac{d^2\hat{p}_1}{dx^2} + b_1\left(\frac{dp_1}{dx}\right)^2 + b_o = 0 \tag{2.133}$$

where $\hat{p}_1(x)$ is the steady state first-order pressure perturbation; the coefficients are:

$$b_0 \equiv \frac{F_0/\overline{B}_0}{K_u/V_0} \qquad b_1 \equiv \frac{F_0/\overline{B}_0}{\gamma P_0} \tag{2.134}$$

Note that at steady state, according to Eqs. (2.107) and (2.112), respectively, $C_0=F_0$ and $C_1=F_0v_0$; thus, in Eq. (2.132), $C_1-C_0v_0=0$.

The boundary data are,

$$dp_1/dx(0)=0, \qquad \text{and } p_1(x=L)=p_L \tag{2.135}$$

The solution is straightforward,

$$d\hat{P}_1/dx = -\sqrt{b_0/b_1}\, tg\left(\sqrt{b_0 b_1}\, x\right) \tag{2.136}$$

$$\hat{P}_1(x) = \hat{P}_1^0 + \frac{1}{b_1} \ln\left|\cos\sqrt{b_0 b_1}\, x\right| \tag{2.137}$$

This concludes the derivation of the injected, viscous wall layer, up to second order. Full solutions, namely, matching between inner and outer expansions will not be attempted herein. Important insights are obtained already from resolving the near-field behavior up to second order, in terms of the y-polynominals.

2.3.3 DISCUSSION OF RESULTS

To facilitate comparison with the experimental data reported by Brown, et al, one may form the normalized axial pressure differential,

$$\Delta p_1 \equiv \Delta\hat{p}_1/\varepsilon\hat{p}_o = \frac{1}{\varepsilon\hat{p}_o}\left[\hat{p}(x=0) - \hat{p}(x)\right] =$$
$$= \frac{1}{\varepsilon\hat{p}_o}\left\{(\hat{p}_o + \varepsilon\hat{p}_1^o) - (\hat{p}_o + \varepsilon\hat{p}_1^o + \frac{\varepsilon}{b_1}\ln|\cos\sqrt{b_o b_1}\,x|)\right\} =$$
$$= \frac{1}{b_o\hat{p}_o}\ln|\cos\sqrt{b_o b_1}\,x| \qquad (2.138)$$

This axial pressure differential expression is used to correlate the experimental data of Brown, et al, as shown in Fig. 4. Clearly, the measured pressure profile is correlated very well by Eq. (2.138), which is obviously superior to the expression attributed to Culick, shown as well.

It should be pointed out that a single point of the data (x; p_1) has been utilized to obtain a scale for the comparison (this is necessary, since no physical input is available regarding the value of B_o, the perturbed injected mass flux, necessary for defining b_1, b_o), along with $p_o=F_o = v_o = 1$, and $\gamma = 1.4$. Suppose now that $K_m=1$, and we select a value of $B_o=60$. (This is based on some trial and error - but shows how the correlation was obtained without any regression analysis); then,

$$b_o=1/B_o=1/60, \quad b_1=1/\gamma B_o=1/1.4\text{x}60, = 0.012$$
$$\sqrt{b_o b_1} = 1/\sqrt{\gamma}\,B_o = 0.014$$

Two important observations are therfore demonstrated: (1) axial pressure variation to lowest order is $O(\varepsilon)$, and is **governed by the dissipative wall layer processes,** as shown in the rigorous analysis herein. The behavior obtained in x differs from the parabolic pressure drop formula of Culick [1], and (2) one need not invoke local turbulence generation or turbulence encroachment upon the surface to explain the departure of measured Δp_1 from a laminar behavior.

Another property of interest is the wall friction coefficient, or dimensionless wall shear stress,

$$C_f = \tau_\omega^*/\tfrac{1}{2}\rho^*\bar{u}^{*2} = -\mu^*\frac{\partial u^*}{\partial y^*}(y=0)/\tfrac{1}{2}\rho^*\bar{u}^{*2}$$

where $\bar{u}^*$ denotes the mean axial coreflow velocity. Using dimensionless convention employed herein, along with the wall layer coordinate,

$$C_{fo} = -\varepsilon\,\frac{\partial u_o/\partial y}{\partial x^2}, \qquad (2.139)$$

as $\bar{u}=2x$ was used, for a cylindrical port, and subscript zero denotes zeroth order convention.

Now, from Eqs. (47) and (77),

$$C_{f0} \doteq -\varepsilon \frac{K_u}{F_0} \frac{\partial P_1}{\partial x} / 2x^2 = \varepsilon \left(\frac{K_u}{F_0} \frac{\gamma P_0}{\rho_0} \right)^{1/2} \cdot \frac{tg(\sqrt{b_0 b_1}\, x)}{2x^2} . \qquad (2.140)$$

where the first square root term is of order unity. This parameter is plotted against 1/2x (which denotes the ratio of blowing to mean axial velocity) in Fig. 5. A nearly linear relationship is obtained, using the foregoing coefficient values. In comparison, the data obtained by Olson and Eckert [6] is considered. Ref. 6 includes a plot of the ratio of (axial pressure gradient)/(mean dynamic axial head) vs $v_0^*/\bar{u}_0^* = 1/2x$. This obtains an almost linear correlation, as would be expected from a parabolic pressure drop. The slight curvature however, particularly apparent at small values of $1/2x < 0.01$, can be followed only with the present formulation, not with any parabolic pressure profile. Thus, the first order pressure distribution, obtained from the viscous wall layer analysis, agrees well with the measured data of Brown, et al [8], while the associated wall friction coefficient follows the same trend as that measured by Olson and Eckert [6].

2.3.4 CONCLUSIONS

A derivation of the viscous wall layer regime has been presented, pertaining to the injected flow in an axial porous tube, in simulation of interior solid propellant rocket flows.

Solutions for the radial coordinate (or y-dependence) of all the dependent variables up to the second order have been generated, in polynominal form. The (x,t)-dependence is defined in terms of a relatively simple partial differential system.

Particular results of the analysis for the special case of steady state are: (1) the first order pressure perturbation was solved for and its axial distribution is given explicitly; this term is entirely due to the laminar dissipative wall-layer processes, and (2) the blown wall friction coefficient was likewise defined. Both results correlate well the available experimental data. Finally, (3) the zeroth order axial velocity distribution within the layer is linear radially; thus, to lowest order, viscous dissipation is negligible in the axial momentum balance. This indicates why inviscid, rotational solutions (such as those of Culick [1] and others, chosen so as to satisfy the no-slip condition at the wall) are so successful in representing this family of flows - up to first order.

REFERENCES

1. Culick,F.E.C., "Rotational, Axisymmetric Mean Flow and Damping of Acoustic Waves in a Solid Propellant Rocket", AIAA Journal, Vol 4, No. 8, August 1966, pp. 1462-1464.

2. Berman, A.S., "Laminar Flow in Channels with Porous Walls", Journal of Applied Physics, Vol. 24, No. 9, September 1953, pp. 1232-1235.

3. Sir Geoffrey Taylor, "Fluid Flow in Regions Bound by Porous Surfaces", Proc. Royal Soc. of London, Ser. A., Vol. 234, No. 1199 (1956), pp. 456-475.

4. Wageman, W.E., and Guevara, F.A., "Fluid Flow Through a Porous Channel", The Physics of Fluids, Vol. 3, No. 6, November-December 1960, pp. 878-881.

5. Dunlap, R., Willoughby, P.G., and Hermsen, R.W., "Flowfield in the Combustion Chamber of a Solid Propellant Rocket Motor", AIAA Journal, Vol. 12, No. 10, October 1974, pp. 1440-1442.

6. Olson, R.M., and Eckert, E.R.G., "Experimental Studies of Turbulent Flow in a Porous Circular Tube with Uniform Fluid Injection Through the Tube Walls", Jour. of Appl. Mech./ Transactions of the ASME, March 1966, pp. 7-17.

7. Huesman, K., and Eckert, E.R.G., "Studies of the Laminar Flow and Transition to Turbulence in Porous Tubes, with Uniform Injection Through the Tube Wall", (Translation), Warme und Stoffubertrannung, Bd. 1 (1968), pp. 2-9.

8. Brown, R.S., Waugh, R.C., Willoughby, P.G., and Dunlap, R., "Coupling Between Velocity Oscillations and Solid Propellant Combustion", 19th JANNAF Combustion Meeting, October 1982, CPIA Publication 366, Vol. I, pp. 191-208.

9. Yagodkin, V.I., "Use of Channels with Porous Walls for Studying Flows Which Occur During Combustion of Solid Propellants", Proc. 18th Aeronautics Congress, Vol. 3, 1967, pp. 69-79. (Trans.)

10. Yamada, K. Goto, M., and Ishikawa, N., "Simulative Study on the Erosive Burning of Solid Rocket Motors", AIAA Journal, Vol. 14, No. 9, September 1976, pp. 1170-1177.

11. Varapaev, V.N. and Yagodkin, V,I., "Flow Instability in a Channel with Porous Walls", AN, SSSR, Mekhanika Zhidkosti i Gaza, Vol. 4, No. 5, pp. 91-95, 1969. (Trans.)

12. Sviridenkov, A.A., and Yagodkin, V.I., "Flow in the Initial Sections of Channels with Permeable Walls", Izv. AN, SSSR, Mekhanika Zhidkosti i Gaza, No. 5, pp. 43-48, September-October 1976 (Moscow). (Trans.)

13. Goldshtik, M.A., and Sapozhnikov, V.A., "Laminar Flow Stability in a Mass Force Field", lzv. AN. SSSR, Mekhanika Zhidkosti i Gaza, Vol. 3, No. 5, pp. 42-46, 1968.

14. Alekseev, Yu. N., and Korotkin, A.I., "Effect of Transverse Stream Velocity in an Incompressible Boundary Layer on the Stability of the Laminar Flow Regime", Mekhanika Zhidkosti i Gaza, Vol. 1, No. 1, pp. 32-36, 1966.

15. Flandro, G.A., "Nonlinear Time Dependent Combustion of a Solid Rocket Propellant", Proc. 19th JANNAF Combustion Meeting, October 1982, CPIA Publication 366, Vol. II, pp. 111-122.

16. T'ien, J., "Oscillatory Burning of Solid Propellants including Gas Phase Time Lag", Combustion Science and Technology", Vol. 5, 1972, pp. 47-54.

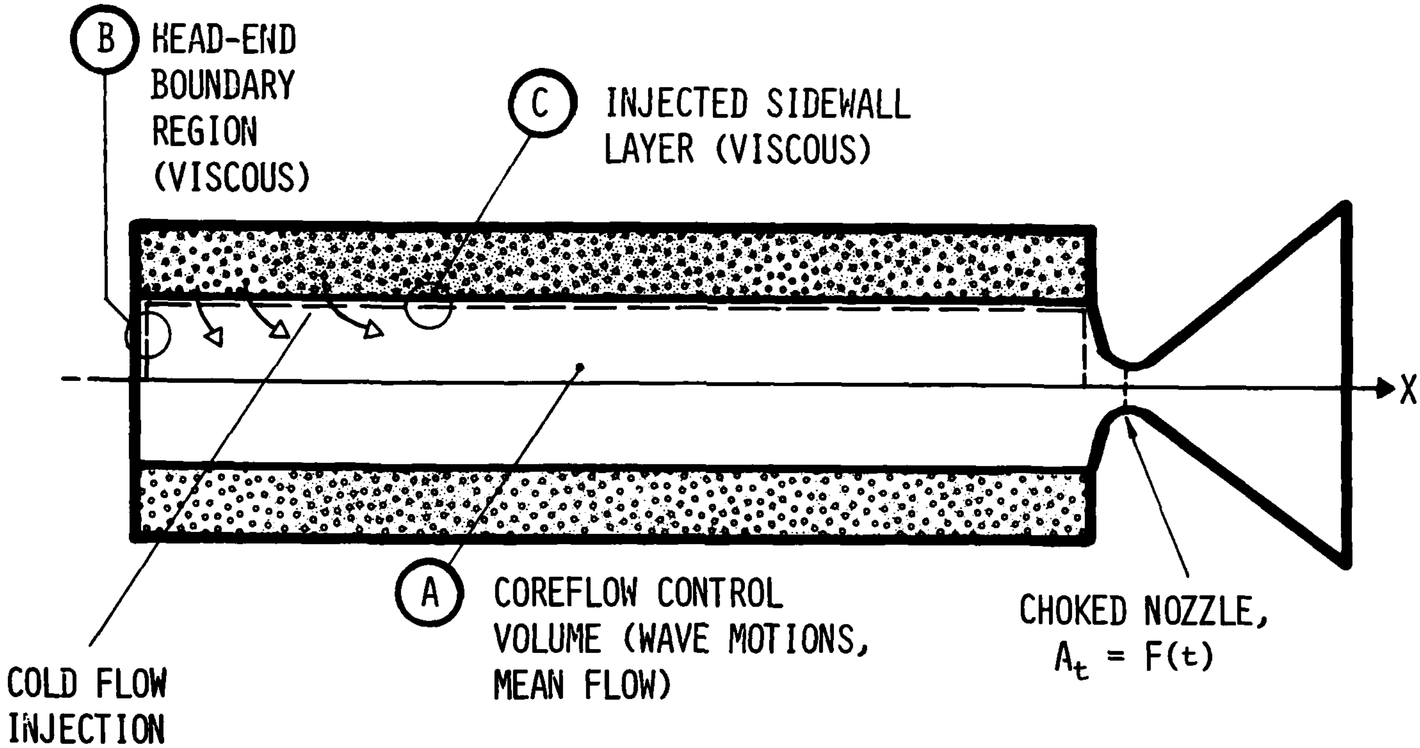

FIGURE 2.1 SIMULATED (AXISYMMETRIC, NONSTEADY) ROCKET CHAMBER FLOW, SHOWING THE 3 SPECIFIC REGIONS OF INTEREST IN THE PRESENT ANALYSIS.

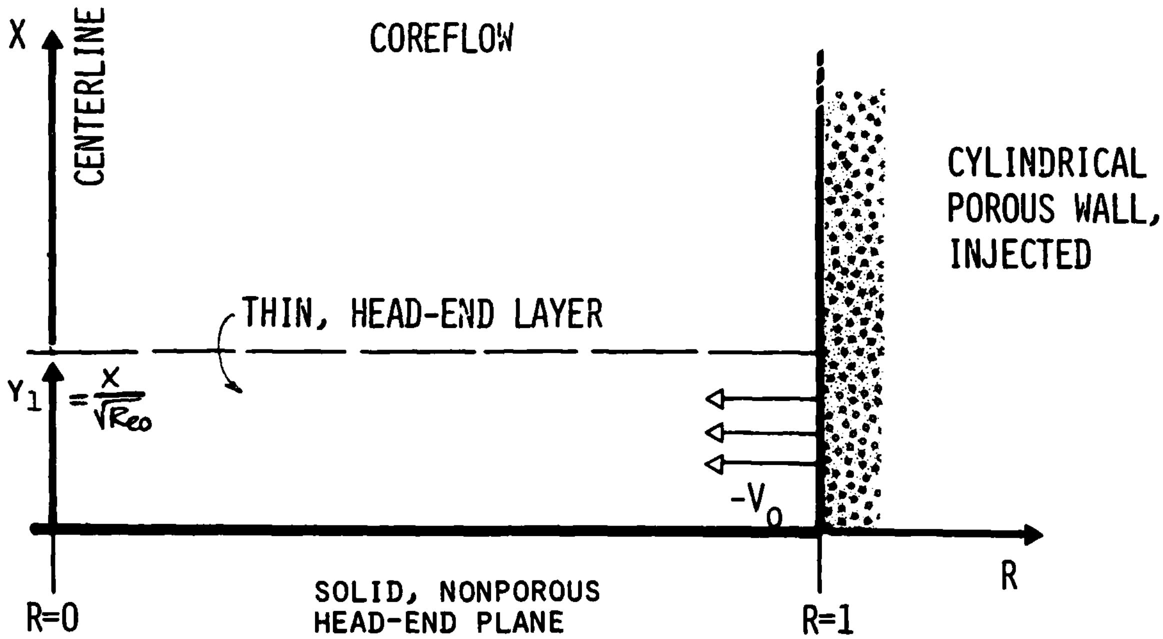

FIGURE 2.2 SCHEMATIC OF THE HEAD-END LAYER, WITH THE STRETCHED AXIAL COORDINATE.

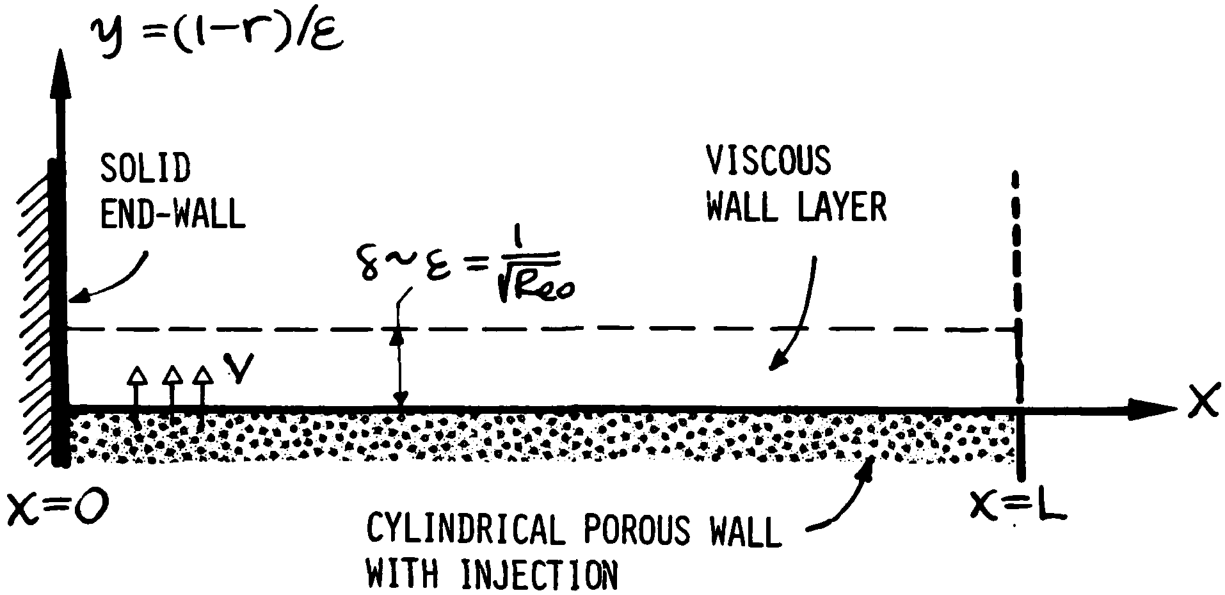

FIGURE 2.3 SCHEMATIC OF THE INJECTED WALL-LAYER REGION WITH THE PERTURBED (EXPANDED) COORDINATE. (THE "COREFLOW" REGIME IS ABOVE, TOWARD THE CENTERLINE.)

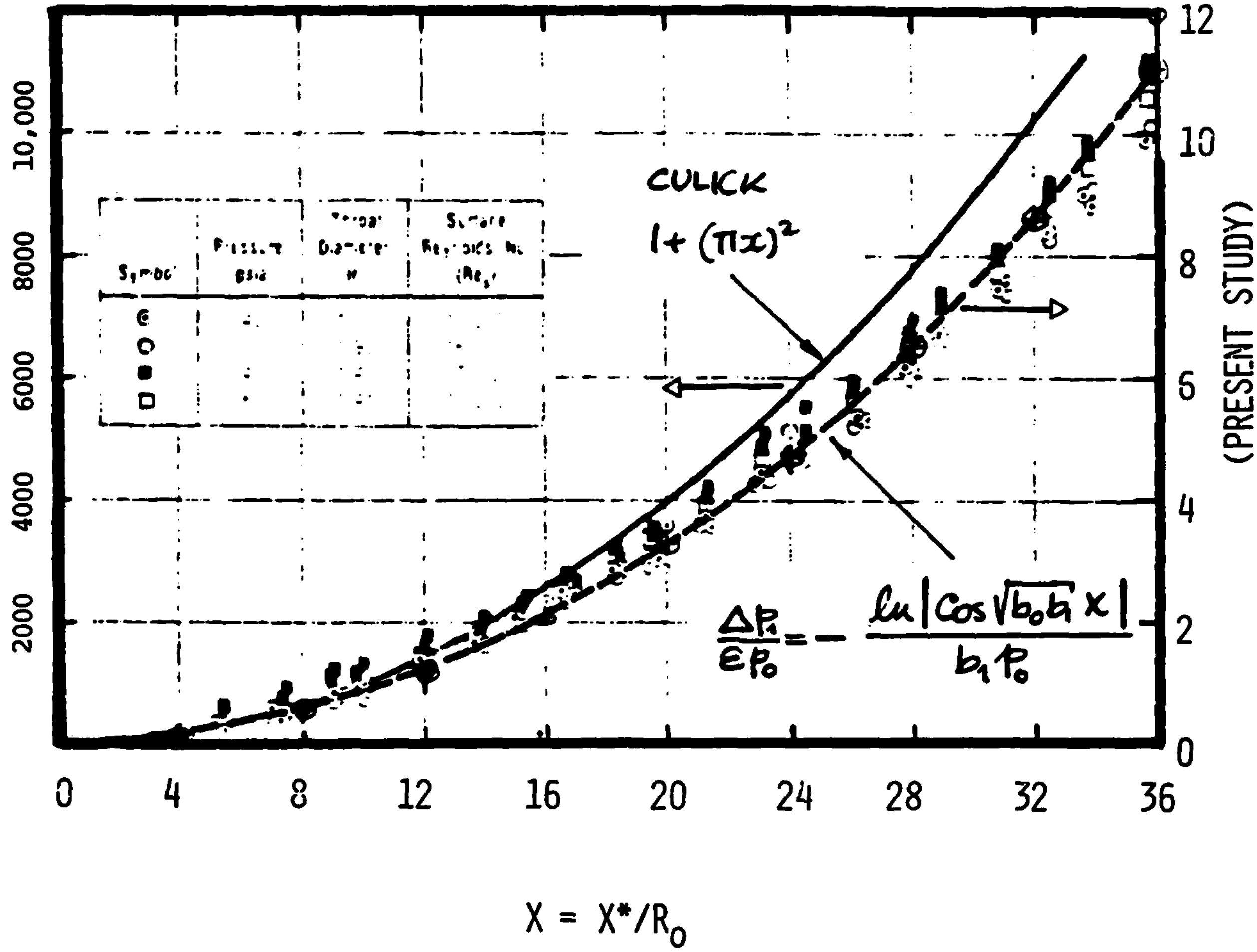

FIGURE 2.4 DIMENSIONLESS FIRST ORDER AXIAL PRESSURE DISTRIBUTION, FROM THE NEAR-FIELD ANALYSIS HEREIN. THE CURRENT RESULT IS PLOTTED OVER THE ORIGINAL FIGURE OF CSD/UTC (1982), WHICH ALSO SHOWS THE PARABOLIC FORMULA OF CULICK.

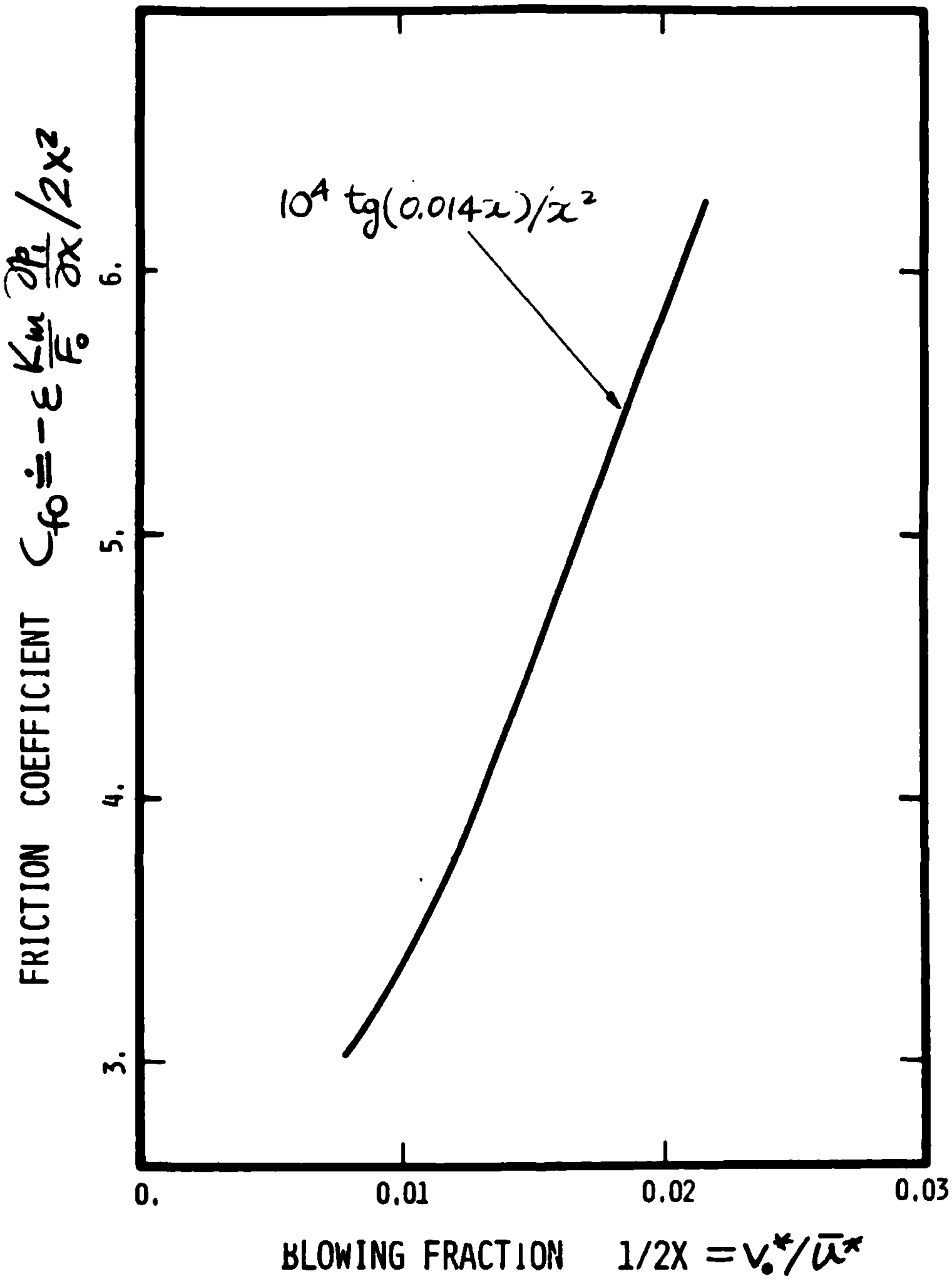

FIGURE 2.5 WALL FRICTION COEFFICIENT, FROM FIRST ORDER NEAR-FIELD ANALYSIS HEREIN. THE SLIGHT CURVATURE OCCURS ALSO IN THE EXPERIMENTAL RESULTS OF OLSON AND ECKERT (1966); ADJUSTMENT WAS NOT ATTEMPTED.

NOMENCLATURE

A_t, A	= nozzle throat area and port exit area, respectively
a	= adiabatic velocity of sound
C_f	= wall friction coefficient, Eq. (2.139)
C_v, C_p	= isochoric and isobaric specific heats (J/kg-K)
F	= radial mass flux (dimensionless)
G	= axial mass flux (dimensionless)
h	= thermal enthalpy, dimensionless
K_m	= ratio of inverse Reynolds number and Mach number squared, Eq. (2.30), (2.76)
L	= chamber length
M	= Mach number
p	= pressure
P_r	= Prandtl number, Eq. (2.8)
R_o*	= channel radius
R_{eo}	= injected Reynolds number, Eq. (2.7)
r	= radial coordinate
$S_{1,2,3}$	= "source"-terms in the equations of motion for coreflow, Eqs. (2.13)-(2.15)
S_{RO}	= Strouhal number, injected, (Eq. 2.34)
t	= time (dimensionless)
U_o	= parameter defining (x,t) - variation of wall layer axial velocity component
u, u	= axial velocity, and mean axial coreflow velocity respectively
v	= radial velocity component
x	= axial distance (dimensionless)
y	= radial, magnified wall layer coordinate, perpendicular to surface, Eq. (2.72)
y_1	= axial magnified coordinate (head-end boundary layer), Eq. (2.25)

Greek Symbols:

γ	= C_p/C_v specific heat ratio
Δ	= difference, increment, Eq. (2.138)
δ	= length scales, Eqs. (2.31)-(2.34)
ε	= small perturbation quantity, Eqs. (2.24); (2.73)
λ	= thermal conductivity of gas (air), J/K-m-s
μ	= viscosity coefficient, kg/m-s
ρ	= density

Subscripts, Superscripts:

$(\ )_o$	= denotes zeroth order (perturbation)
$(\ )_1$	= denotes first order perturbation
$(\ )^*$	= denotes dimensional quantity

3. NUMERICAL SIMULATION

A comprehensive numerical algorithm has been derived an implemented for simulation of the axisymmetric, nonsteady internal flow field.

The finite difference method used is a modified MacCormack explicit algorithm [1], utilizing the original predictor-corrector scheme. Unlike the original MacCormack algorithm, which utilizes split time marching [2], the present scheme is unsplit (namely, both radial and axial space derivatives are taken into acount at each internal predictor-step, within a single overall time increment). This affords better stability, particularly near the walls [3].

The initial spatial discretization scheme is shown in Fig. 3.1. Preliminary versions employed uniform radial mesh size, to save computation time in marching toward steady state from some artificial state described by the initial data. Since the time marching is explicit, the smallest spatial increment must obviously be used in the Courant-Friedrichs-Lewy condition,

$$c \cdot \Delta t / \Delta R_{min} < 1$$

where $c = a + V_{max}$ is the dimensionless maximal, local characteristic slope.

The foregoing drawback due to stability requirements is marginal compared with the great advantage (at least in terms of the coreflow region simulation), when compared with implicit methods which would require much more CPU-core space for setup and execution.

The algorithm uses the dimensionless equations of motion in conservation form, as shown in the preceding Section. It is written in FORTRAN IV and operated on a DECK mini computer. A schematic of the program morphology is given by the block diagram of Fig. 3.2. A preliminary listing is provided in Appendix A.

REFERENCES

1. MacCormack, R.W., and Paullay, A.J., "The Influence of the Computational Mesh on Accuracy for Initial Value Problems with Discontinuous or Nonunique Solutions", Computers & Fluids, Vol. 2, 1974, pp. 339-361.

2. Marchuk, G.I., "The Theory of Splitting Up Method", Numerical Solutions of Partial Differential Equations-II, SYNSPADE 1970, Ed. Bert Hubbard, Acad. Press, N.Y., 1971, pp. 469-500.

3. Drummond, J.P. (NASA Langley Research Center), Personal Communication, September 1983.

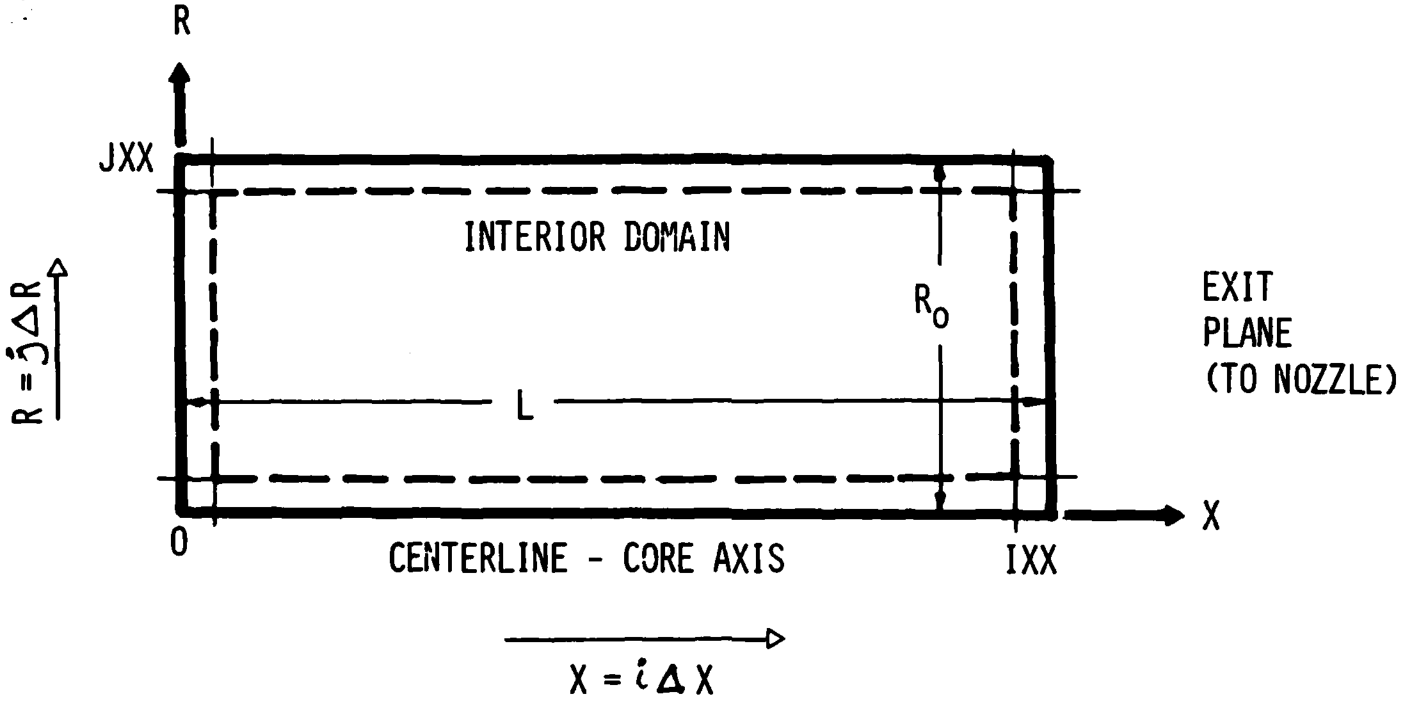

TYPICAL VALUES: JXX = 10, IXX = 25, RØ = 1, L = 25.

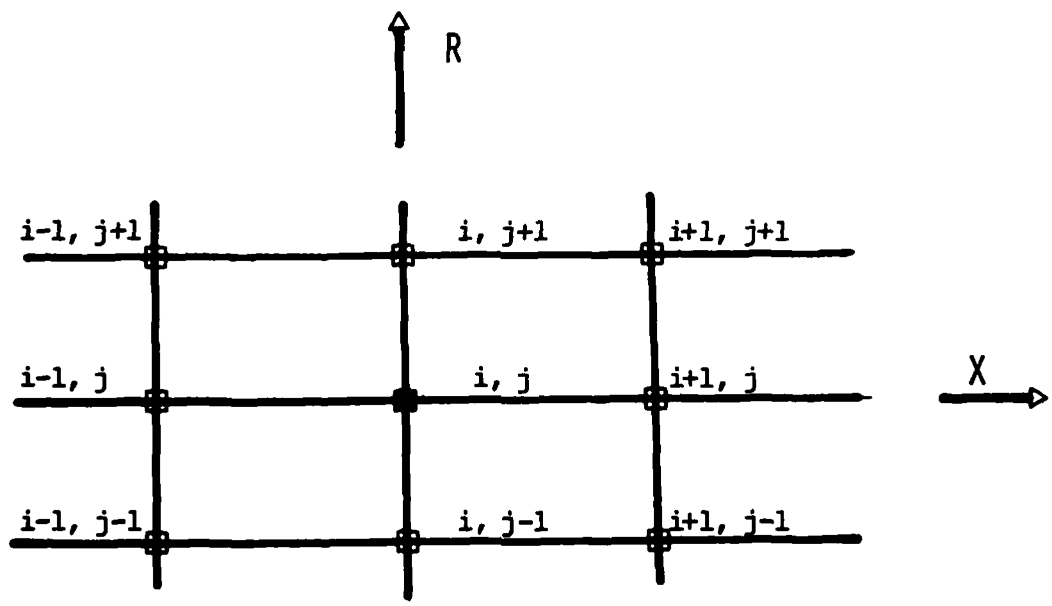

FIGURE 3.1 COMPUTATIONAL MESH FOR AXISYMMETRIC COREFLOW SIMULATION

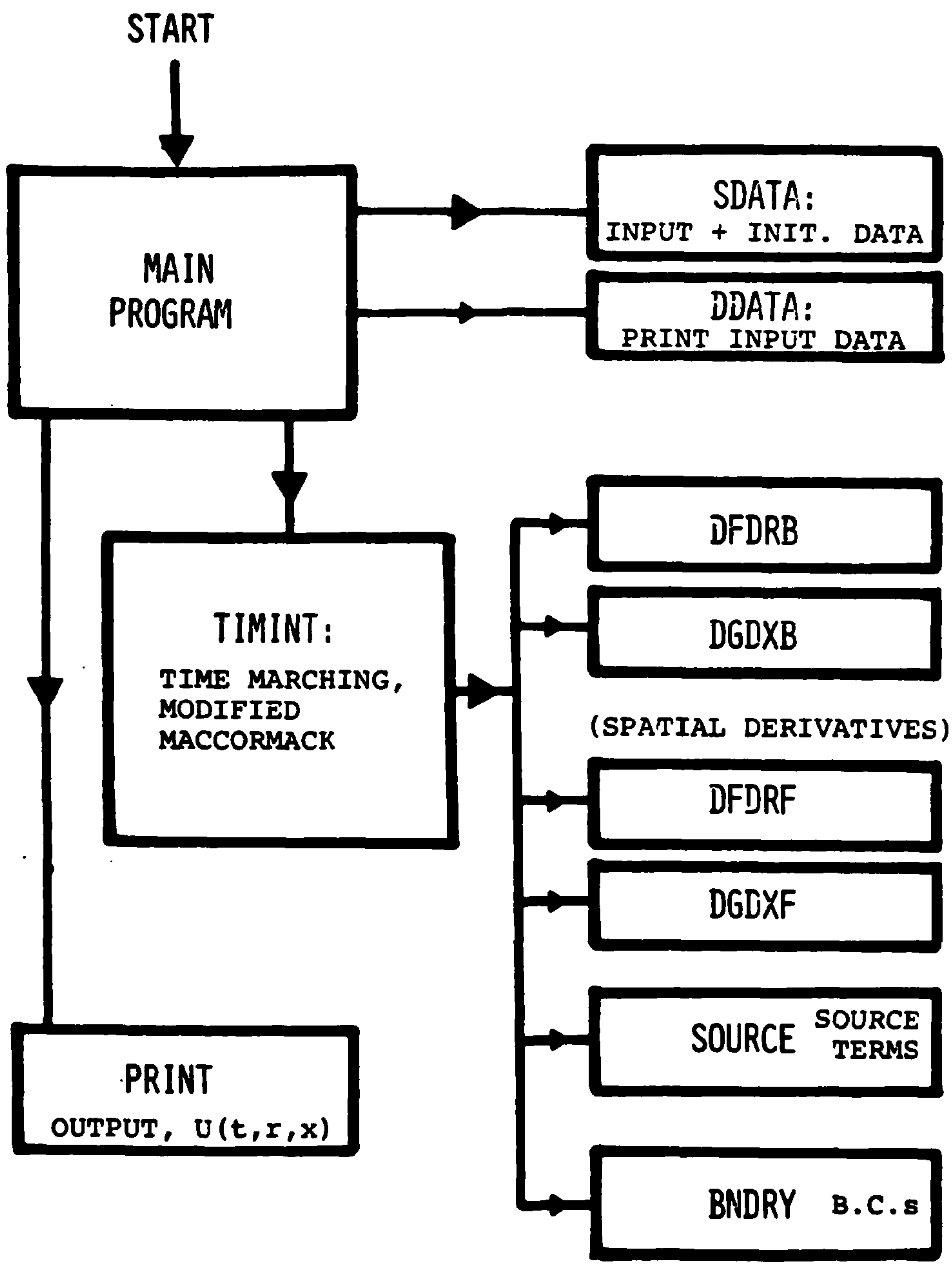

FIGURE 3.2 BLOCK DIAGRAM FOR AXISYMMETRIC NONSTEADY COREFLOW SIMULATION CODE

APPENDIX A

```
C INTEGRATION BY MAC CORMACK METHOD
C TWO DIMENSIONAL SIMULATION IN R-X

C U(1,J,K)=RHOG=DENSITY OF GAS
C U(2,J,K)=RADIAL MOMENTUM=RHOG * RADIAL VELOCITY
C U(3,J,K)=AXIAL MOMENTUM=RHOG * AXIAL VELOCITY
C U(4,J,K)=THERMAL ENTHALPY=RHOG * ENTHALPY

C JXX=NUMBER OF RADIAL DIVISIONS
C KXX=NUMBER OF AXIAL DIVISIONS
C JXM1=JXX-1
C KXM1=KXX-1

C GAMA, REYNOLDS NUMBER, PRANDTL NUMBER, AND MACH NUMBER:
C GAMA=RATIO OF SPECIFIC HEAT=CP/CV
C REO=REYNOLDS NUMBER=RHOG * VZERO * RSTAR / VISC
C PRN=PRANDTL NUMBER=VISC * CP / COND
C EMO=MACH NUMBER=VZERO / SSND
C EMO2=MACH NUMBER SQUARE=EMO ** 2
C CFL=COURANT-FRIEDRICHS-LEWY NUMBER

C NOTE: ALL UNITS IN S.I - MKS
C VZERO=REFERENCE INJECTION VELOCITY .........................,M/SEC
C RHOG=REFERENCE GAS DENSITY ..................................,KG/M**3
C RSTAR=MOTOR DIAMETER(INNER) .................................,M
C XSTAR=MOTOR LENGTH ..........................................,M
C PSTAR=GAS PRESSURE ..........................................,N/M**2
C VISC=COEFFICIENT OF VISCOSITY OF GAS ........................,KG/M-SEC
C CP=SPECIFIC HEAT OF GAS(ISOBAR) .............................,JOULE/K-KG
C COND=COEFFICIENT OF THERMAL CONDUCTIVITY OF GAS .............,JOULE/K-M-SEC
C SSND=SPEED OF SOUND=(GAMA*PSTR/RHOG)**0.5 ...................,M/SEC

C        MAIN PROGRAM

         DIMENSION U(4,5,10),RR(5)
         COMMON/BLOCK1/GAMA,CG1,DR,DX,JXM1,KXM1,MXM1,JXX,KXX,MXX
         COMMON/BLOCK2/REO,PRN,GAM1,CG2,CG3,CG4,CG5,TODR,TODX,DR2,DX2,RR
         COMMON/BLOCK3/U,DT
         COMMON/BLOCK4/RSTAR,RO,XSTAR,XO,VSTAR,VO,PSTAR,PO,RHOG,SSND,EMO
      *  ,CFL

         TIME=0.
         ITMAX=2
         CALL SDATA
C        DT=1.E-5
         CALL PDATA
         DO 5 L=1 , ITMAX
         CALL TIMINT(U,TIME,DT)
         CALL PRINT(U,TIME)
    5    CONTINUE

         STOP
         END
```

```
      SUBROUTINE TIMINT(U,TIME,DT)

      DIMENSION U(4,5,10),UB(4,5,10),DF(4,5,10),DG(4,5,10),S(4,5,10),
     * SB(4,5,10),RR(5)
      COMMON/BLOCK1/GAMA,CG1,DR,DX,JXM1,KXM1,MXM1,JXX,KXX,MXX
      COMMON/BLOCK2/REO,PRN,GAM1,CG2,CG3,CG4,CG5,TODR,TODX,DR2,DX2,RR

C 2-STEP,2-DIMENSIONAL MAC CORMACK METHOD
      CALL DFDRB(U,DF)
      CALL DGDXB(U,DG)
      CALL SORCE(U,S)
      DO 600 M=1,MXX
      DO 600 J=2,JXM1
      DO 600 K=2,KXM1
      UB(M,J,K)=U(M,J,K)-DT*DF(M,J,K)-DT*DG(M,J,K)+DT*S(M,J,K)
600   CONTINUE
C
      DO 603 M=1,MXX
      DO 603 K=1,KXX
      UB(M,JXX,K)=U(M,JXX,K)
603   UB(M,1,K)=U(M,1,K)
      DO 604 M=1,MXX
      DO 604 J=2,JXM1
      UB(M,J,KXX)=U(M,J,KXX)
604   UB(M,J,1)=U(M,J,1)
C
      CALL BNDRY(UB)

      CALL DFDRF(UB,DF)
      CALL DGDXF(UB,DG)
      CALL SORCE(UB,SB)
      DO 605 M=1,MXX
      DO 605 J=2,JXM1
      DO 605 K=2,KXM1
      U(M,J,K)=0.5*(U(M,J,K)+UB(M,J,K))-DT/2.*DF(M,J,K)-DT/2.
     * *DG(M,J,K)+DT/4 *(S(M,J,K)+SB(M,J,K))
605   CONTINUE
C
      CALL BNDRY(U)

      TIME=TIME+DT
      RETURN
      END
```

```
C
      SUBROUTINE SDATA
C
      DIMENSION U(4,5,10),RR(5)
      COMMON/BLOCK1/GAMA,CG1,DR,DX,JXM1,KXM1,MXM1,JXX,KXX,MXX
      COMMON/BLOCK2/REO,PRN,GAM1,CG2,CG3,CG4,CG5,TODR,TODX,DR2,DX2,RR
      COMMON/BLOCK3/U,DT
      COMMON/BLOCK4/RSTAR,RO,XSTAR,XO,VZERO,VO,PSTAR,PO,RHOG,SSND,EMO
     * ,CFL
C PROBLEM DATA AND BOUNDARY VALUES
      VZERO=1.0
      RHOG=1.24
      VISC=1.E-5
      CP=1.16E3
      COND=1.66E-2
      PSTAR=2.E5

      RSTAR=0.05
      XSTAR=0.25
      GAMA=1.4
      SSND=(GAMA*PSTAR/RHOG)**0.5
C DIMENSIONLESS GROUP
      CFL=0.8
      GAMA=1.4
      REO-RHOG*VZERO*RSTAR/VISC
      PRN=VISC*CP/COND
      EMO=VZERO/SSND
      EMO2=EMO**2
C
      VO=1.
      PO=1.
      RO=1.
      XO=XSTAR/RSTAR
C
      GAM1=GAMA-1.
      GAM2=GAM1/GAMA
      GAM3=GAMA+EMO2
      CG1=GAM2/GAM3
      CG2-4./3./REO
      CG3=1./REO
      CG4=GAMA/REO/PRN
      CG5=GAM1*GAM3/REO
C MESH=5*9
      JXX=5
      KXX=9
      MXX=4
      JXM1=JXX-1
      KXM1=KXX-1
      MXM1=MXX-1
C
      DR=RO/JXM1
      DX=XO/KXM1
      TODR=2.*DR
      TODX=2.*DX
      DR2-DR*DR
      DX2-DX*DX
```

```
C TIME INCREMENT CALCULATION

C 1. THE COURANT-FRIEDRICHS-LEWY NUMBER=CFL, STATES THAT C*DT/DX .LE. CFL
C WHERE C=CHARACTERISTIC VELOCITY, AND CFL .GT. 0 AND .LE. 1. CFL IS AN INPU

C 2  DT=THE DIMENSIONLESS TIME INCREMENT, ACCORDING TO THE CFL CONDITION.
C ONE HAS TO CHOOSE THE SMALLEST (MIN. OVER K,J) ONE:
C                   DTXX=CFL*DX/CX
C                   DTRR=CFL*DR/CR

C
          ENX=XO/RO
          UMAX=2.*ENX
          CX=UMAX+1./EMO
          CR=1.+1./EMO

          DTXX=CFL*DX/CX
          DTRR=CFL*DR/CR
          DT=AMIN1(DTXX,DTRR)


C
          U10=1.
          U20=1.
          U30=1.
          U40=GAMA/(GAMA-1)
C
          DO 701 J=2,JXX
701       RR(J)=DR*(J-1)

C INITIAL VALUE

C J=1
          DO 700 K=1,KXX
          U(1,1,K)=U10
          U(2,1,K)=0.
          U(3,1,K)=U10*2.*DX*(K-1)
          U(4,1,K)=U40
C J=JXX
          U(1,JXX,K)=U10
          U(2,JXX,K)=U20
          U(3,JXX,K)=0.
          U(4,JXX,K)=U40
700       CONTINUE
C K=1
          DO 705 J=2,JXX
          U(1,J,1)=U10
          U(2,J,1)=0.
          U(3,J,1)=0.
          U(4,J,1)=U40
705       CONTINUE
```

```
C K=KXX
        DO 706 J=2,JXM1
        U(1,J,KXX)=U10
        U(2,J,KXX)=U20
        U(3,J,KXX)=U10*2.*DX*KXM1
        U(4,J,KXX)=U40
706     CONTINUE
C INNER POINTS
        DO 710 J=2,JXM1
        DO 710 K=2,KXM1
        U(1,J,K)=U10
        U(2,J,K)=U20
        U(3,J,K)=U10*2.*DX*(K-1)
        U(4,J,K)=U40
710     CONTINUE

        RETURN
        END

C
        SUBROUTINE PDATA
C
        DIMENSION U(4,5,10)
        COMMON/BLOCK1/GAMA,CG1,DR,DX,JXM1,KXM1,MXM1,JXX,KXX,MXX

        COMMON/BLOCK2/REO,PRN,GAM1,CG2,CG3,CG4,CG5,TODR,TODX,DR2,DX2,RR
        COMMON/BLOCK3/U,DT
        COMMON/BLOCK4/RSTAR,RO,XSTAR,XO,VZERO,VO,PSTAR,PO,RHOG,SSND,EMO
     *  ,CFL

        TIME=0.
        CALL PRINT(U,TIME)
        WRITE(1,1000)RSTAR,RO,XSTAR,XO,VZERO,VO,PSTAR,PO
        WRITE(1,1005)RHOG,SSND,REO,PRN,EMO,GAMA,CFL,DR,DX,DT
1000    FORMAT(1H1,8X,'MOTOR DIAMETER(M)=',F5.2,10X,'RO(DIMENSIONLESS)=',
     *  F5.2/9X,'MOTOR LENGTH(M)=',F5.2,12X,'XO(DIMENSIONLESS)=',F5.2/
     *  9X,'INJECTION VELOCITY(M/SEC)=',F5.2,'  VO(DIMENSIONLESS)=',F5.2
     *  /9X,'GAS PRESSURE(N/M**2)=',E9.2,3X,'PO(DIMENSIONLESS)=',F5.2)
1005    FORMAT(9X,'GAS DENSITY(KG/M**3)=',F5.2/
     *  9X,'SPEED OF SOUND(M/SEC)=',E9.2/
     *  9X,'REO=',E9.2/9X,'PRN=',F5.2/9X,'EMO=',E9.2/9X,'GAMA=',F5.2/
     *  9X,'CFL=',F5.2/9X,'DR=',F6.3/9X,'DX=',F6.3/9X,'DT=',E9.2)

        RETURN
        END
```

```
      SUBROUTINE BNDRY(U)
C
      DIMENSION U(4,5,10)
      COMMON/BLOCK1/GAMA,CG1,DR,DX,JXM1,KXM1,MXM1,JXX,KXX,MXX

      DO 900 M=1,MXX
      DO 900 K=2,KXM1
      U(M,1,K)=U(M,2,K)
900   CONTINUE

      DO 905 M=2,3
      DO 905 J=1,JXM1
      U(M,J,KXX)=U(M,J,KXM1)
905   CONTINUE

      RETURN
      END

C
      SUBROUTINE DFDRB(U,DFB)
C
      DIMENSION U(4,5,10),DFB(4,5,10),F(4,5,10)
      COMMON/BLOCK1/GAMA,CG1,DR,DX,JXM1,KXM1,MXM1,JXX,KXX,MXX

      DO 100 M=1,MXX
      DO 100 J=1,JXM1
      DO 100 K=2,KXM1
      F(1,J,K)=U(2,J,K)
      F(2,J,K)=U(2,J,K)*U(2,J,K)/U(1,J,K)+CG1*U(4,J,K)
      F(3,J,K)=U(2,J,K)*U(3,J,K)/U(1,J,K)
      F(4,J,K)=GAMA*U(2,J,K)*U(4,J,K)/U(1,J,K)
100   CONTINUE

      DO 105 M=1,MXX
      DO 105 J=2,JXM1
      DO 105 K=2,KXM1
      DFB(M,J,K)=(F(M,J,K)-F(M,J-1,K))/DR
105   CONTINUE

      RETURN
      END
```

```
C
      SUBROUTINE DGDXB(U,DGB)
C
      DIMENSION U(4,5,10),DGB(4,5,10),G(4,5,10)
      COMMON/BLOCK1/GAMA,CQ1,DR,DX,JXM1,KXM1,MXM1,JXX,KXX,MXX

      DO 200 M=1,MXX
      DO 200 J=2,JXM1
      DO 200 K=1,KXM1
      G(1,J,K)=U(3,J,K)
      G(2,J,K)=U(2,J,K)*U(3,J,K)/U(1,J,K)
      G(3,J,K)=U(3,J,K)*U(3,J,K)/U(1,J,K)+CQ1*U(4,J,K)
      G(4,J,K)=GAMA*U(3,J,K)*U(4,J,K)/U(1,J,K)
200   CONTINUE

      DO 205 M=1,MXX
      DO 205 J=2,JXM1
      DO 205 K=2,KXM1
      DGB(M,J,K)=(G(M,J,K)-G(M,J,K-1))/DX
205   CONTINUE

      RETURN
      END


C
      SUBROUTINE SORCE(U,S)
C

      DIMENSION U(4,5,10),S(4,5,10),V(3,5,10),DVDR(3,5,10),
     * DVDX(3,5,10),DVDR2(3,5,10),DVDX2(3,5,10),DU4DR(5,10),
     * DU4DX(5,10),DVDRDX(2,5,8),RR(5)
      COMMON/BLOCK1/GAMA,CQ1,DR,DX,JXM1,KXM1,MXM1,JXX,KXX,MXX
      COMMON/BLOCK2/REO,PRN,GAM1,CQ2,CQ3,CQ4,CQ5,TODR,TODX,DR2,DX2,RR

C DEFINE V(M,J,K)
      DO 300 M=1,MXM1
      DO 300 J=1,JXX
      DO 300 K=1,KXX
      V(M,J,K)=U(M+1,J,K)/U(1,J,K)
300   CONTINUE

C DEFINE DVDR,DVDR2,DVDX,DVDX2,DVDRDX,DU4DR,DU4DX
      DO 305 M=1,MXM1
      DO 305 J=2,JXM1
      DO 305 K=2,KXM1
      DVDR(M,J,K)=(V(M,J+1,K)-V(M,J-1,K))/TODR
      DVDR2(M,J,K)=(V(M,J+1,K)-2.*V(M,J,K)+V(M,J-1,K))/DR2

      DVDX(M,J,K)=(V(M,J,K+1)-V(M,J,K-1))/TODX
      DVDX2(M,J,K)=(V(M,J,K+1)-2.*V(M,J,K)+V(M,J,K-1))/DX2

305   CONTINUE
```

```
      DO 310 J=2,JXM1
      DO 310 K=2,KXM1
      DVDRDX(1,J,K)=(V(1,J+1,K+1)-V(1,J+1,K-1)-V(1,J-1,K+1)+
     * V(1,J-1,K-1))/TODR/TODX
      DVDRDX(2,J,K)=(V(2,J+1,K+1)-V(2,J+1,K-1)-V(2,J-1,K+1)+
     * V(2,J-1,K-1))/TODR/TODX
      DU4DR(J,K)=(U(4,J+1,K)-U(4,J-1,K))/TODR

      DU4DX(J,K)=(U(4,J,K+1)-U(4,J,K-1))/TODX
310   CONTINUE


C CALCULATE S(M,J,K)
      DO 315 J=2,JXM1
      DO 315 K=2,KXM1
      S(1,J,K)=-U(2,J,K)/RR(J)

      S(2,J,K)=-U(2,J,K)*V(1,J,K)/RR(J)+CG2/RR(J)*(DVDR(1,J,K)-
     * V(1,J,K)/RR(J))+CG3*DVDX2(1,J,K)+CG3*DVDRDX(2,J,K)/3.+
     * CG2*DVDR2(1,J,K)

      S(3,J,K)=-U(3,J,K)*V(1,J,K)/RR(J)+CG3/RR(J)*(DVDR(2,J,K)+
     * DVDR(1,J,K)/3.)+CG3*DVDR2(2,J,K)+CG2*DVDX2(2,J,K)+CG3*
     * DVDRDX(1,J,K)/3

      S(4,J,K)=-GAMA*U(4,J,K)*V(1,J,K)/RR(J)+GAM1*(V(1,J,K)*
     * DU4DR(J,K)+V(2,J,K)*DU4DX(J,K))+CG4*(DVDR(3,J,K)
     * /RR(J)+DVDR2(3,J,K)+DVDX2(3,J,K))+CG5*(4./3.*(DVDX(2,J,K)
     * **2+DVDR(1,J,K)**2+(V(1,J,K)/RR(J))**2)+DVDR(2,J,K)**2
     * +DVDX(1,J,K)**2-4.*(V(1,J,K)/RR(J)*DVDR(1,J,K)+V(1,J,K)/
     * RR(J)*DVDX(2,J,K)+DVDR(1,J,K)*DVDX(2,J,K)))

315   CONTINUE

      RETURN
      END
```

```
      SUBROUTINE DFDRF(U,DFF)
C
      DIMENSION U(4,5,10),DFF(4,5,10),F(4,5,10)
      COMMON/BLOCK1/GAMA,CG1,DR,DX,JXM1,KXM1,MXM1,JXX,KXX,MXX

      DO 400 M=1,MXX
      DO 400 J=2,JXX
      DO 400 K=2,KXM1
      F(1,J,K)=U(2,J,K)
      F(2,J,K)=U(2,J,K)*U(2,J,K)/U(1,J,K)+CG1*U(4,J,K)
      F(3,J,K)=U(2,J,K)*U(3,J,K)/U(1,J,K)
      F(4,J,K)=GAMA*U(2,J,K)*U(4,J,K)/U(1,J,K)
400   CONTINUE

      DO 405 M=1,MXX
      DO 405 J=2,JXM1
      DO 405 K=2,KXM1
      DFF(M,J,K)=(F(M,J+1,K)-F(M,J,K))/DR
405   CONTINUE

      RETURN
      END

C
      SUBROUTINE DGDXF(U,DGF)
C
      DIMENSION U(4,5,10),DGF(4,5,10),G(4,5,10)
      COMMON/BLOCK1/GAMA,CG1,DR,DX,JXM1,KXM1,MXM1,JXX,KXX,MXX

      DO 500 M=1,MXX
      DO 500 J=2,JXM1
      DO 500 K=2,KXX
      G(1,J,K)=U(3,J,K)
      G(2,J,K)=U(2,J,K)*U(3,J,K)/U(1,J,K)
      G(3,J,K)=U(3,J,K)*U(3,J,K)/U(1,J,K)+CG1*U(4,J,K)
      G(4,J,K)=GAMA*U(3,J,K)*U(4,J,K)/U(1,J,K)
500   CONTINUE

      DO 505 M=1,MXX
      DO 505 J=2,JXM1
      DO 505 K=2,KXM1
      DGF(M,J,K)=(G(M,J,K+1)-G(M,J,K))/DX
505   CONTINUE

      RETURN
      END
```

```
C
      SUBROUTINE PRINT(U,TIME)
C
      DIMENSION U(4,5,10)
      COMMON/BLOCK1/GAMA,CG1,DR,DX,JXM1,KXM1,MXM1,JXX,KXX,MXX
      KM=(KXX-1)/2+1
      DO 800 M=1,MXX
      IF(M.EQ.1) GO TO 801
      IF(M.EQ.2) GO TO 802
      IF(M.EQ.3) GO TO 803
C M=4
      WRITE (1,840) TIME
      WRITE(1,845)
      GO TO 804
C M=3
803   WRITE (1,835) TIME
      WRITE (1,845)
      GO TO 804
C M=2
802   WRITE (1,830) TIME
      WRITE (1,845)
      GO TO 804
C M=1
801   WRITE (1,825) TIME
      WRITE (1,845)
804   DO 810 K=1,KXX
      IF (K.EQ.KM) GO TO 805
      WRITE (1,815) (U(M,J,K),J=1,5)
      GO TO 810
805   WRITE (1,820) (U(M,J,K),J=1,5)

810   CONTINUE
800   CONTINUE
815   FORMAT (1X,'.',1X,5(E14.6)/)
820   FORMAT (1X,'X',1X,5(E14.6)/)
825   FORMAT (1H1,1X,'U(1,J,K) : GAS DENSITY VS R AND X,',6X,
     *'TIME=',E10.3//)
830   FORMAT (1H1,1X,'U(2,J,K) : RADIAL MOMENTUM VS R AND X,',6X,
     *'TIME=',E10.3//)
835   FORMAT (1H1,1X,'U(3,J,K) : AXIAL MOMENTUM VS R AND X,',6X,
     *'TIME=',E10.3//)
840   FORMAT (1H1,1X,'U(4,J,K) : THERMAL ENTHALPY VS R AND X,',6X,
     *'TIME=',E10.3//)
845   FORMAT (1X,'.....................................R..............
     *..................'//)
      RETURN
      END
```

END

FILMED

9-84

DTIC